AD A136862

GENERAL ⬢ ELECTRIC

MILITARY ELECTRONIC SYSTEMS OPERATION

TECHNICAL INFORMATION SERIES

Author B. A. Deresh R. J. Anderson	Subject Category Variance Estimation	No. R83EMH003
		Date Nov 1983

Title UNBIASED STAND ALONE OPTIMAL ESTIMATION OF MEASURED POSITION VARIANCE FOR TARGETS WITH VARIABLE AND UNKNOWN MEAN PATHS		

Copies Available at MESO TIS Distribution Center Box 4840 (CSP 4-18) Syracuse, New York 13221	GE Class 1	No. of Pages
	Govt Class Unclassified	98

Summary

⟶ Estimation of rms target position accuracy for a radar is of great importance to radar manufacturers and customers alike. With increasing frequency customers insist on direct measurement with small RCS aircraft on radial flight paths. Too often, however, a colocated precision reference radar is unavailable from which to accurately define the true target flight path. In these cases the total error can be tested in two parts: the bias component can be estimated from static measurements and the random component (jitter and thermal error) is estimated as a variance. Here the true target flight path is traditionally modelled as entirely radial. Unfortunately, even small deviations from a true radial can lead to large errors in variance estimation, particularly when the target is close to the radar where the radar error is expected to be small. If the customer requires proof of theoretical accuracy then the model error can be larger than the radar error and the radar will falsely fail the test.

The approach to variance estimation developed here is to estimate the mean target path along with the tri-coordinate position variance and thus avoid the error associated with assuming a simple flight path model. The method is quite general to sensors and targets of all types even though the specific application it was developed for was a radar under test with an aircraft on a radial path. The mean path is assumed to be a sum of orthogonal polynomials of order M. it is shown that so long as M is greater than or equal to K, the effective true order of the mean path (overfitting), that the variance estimate is unbiased in the mean. Moreover the adjacent-point correlation coefficient is shown to be a sensitive indicator of overfitting. The method is shown to be practical in the face of simulation and real flight data even with missing data points as from missed detections. In addition to unbiased optimal estimation of variance, expressions are developed for the uncertainty in the estimate and related to the producer's and consumer's risks of falsely failing or falsely passing a tri-coordinate position accuracy test. Considerable development is accorded sound test design with these principles, and expressions are developed for confidence limits to infer bounds or true variance given the test results.

DTIC FILE COPY

DTIC ELECTE JAN 1 3 1984

Send to _____

A

84   01   13   001

GENERAL ELECTRIC COMPANY TECHNICAL INFORMATION

Within the limitations imposed by Government data export regulations and security classifications, the availability of General Electric Company technical information is regulated by the following classifications in order to safeguard proprietary information:

CLASS 1: GENERAL INFORMATION

Available to anyone on request.
Patent, legal and commercial review required before issue.

CLASS 2: GENERAL COMPANY INFORMATION

Available to any General Electric Company employee on request.
Available to any General Electric Subsidiary or Licensee subject to existing agreements.
Disclosure outside General Electric Company requires approval of originating component.

CLASS 3: LIMITED AVAILABILITY INFORMATION

Original Distribution to those individuals with specific need for information.
Subsequent Company availability requires originating component approval.
Disclosure outside General Electric Company requires approval of originating component.

CLASS 4: HIGHLY RESTRICTED DISTRIBUTION

Original distribution to those individuals personally responsible for the Company's interests in the subject.
Copies serially numbered, assigned and recorded by name.
Material content, and knowledge of existence, restricted to copy holder.

GOVERNMENT SECURITY CLASSIFICATIONS, when required, take precedence in the handling of the material. Wherever not specifically disallowed, the General Electric classifications should also be included in order to obtain proper handling routines.

GENERAL ELECTRIC COMPANY
MILITARY ELECTRONIC SYSTEMS OPERATIONS
TECHNICAL INFORMATION SERIES

SECTION _____ Engineering Operations

UNIT _____ Radar Systems Engineering

MESC ACCOUNTING REFERENCE _____ 510

COLLABORATORS _____ Dr. B. A. Deresh and R. J. Anderson

APPROVED _____ R. L. Benfey _____ TITLE _____ Mgr., RSE _____ LOCATION _____ CSP 5-C4, Syracuse, NY

MINIMUM DISTRIBUTION - Government Unclassified Material (and Title Pages) in G.E. Classes 1, 2, or 3 will be the following.

Copies	Title Page Only	To
0	1	Legal Section, MESO (Syracuse)
0	1	Manager, Technological Planning, MESO (Syracuse)
5	6	G-E Technical Data Center (Schenectady)

MINIMUM DISTRIBUTION - Government Classified Material, Secret or Confidential in G.E. Classes 1, 2, or 3 will be the following.

1	0	Manager, Technological Planning, MESO (Syracuse)

ADDITIONAL DISTRIBUTION (Keep at minimum within intent of assigned C.E. Class.)

COPIES	NAME	LOCATION
5 (CLASS 1 ONLY)	DEFENSE DOCUMENTATION CENTER	CAMERON STATION, ALEXANDRIA, VA. 22314
1	L. I. Chasen	P.O. Box 8555 Philadelphia, Pa., 19101
1	A. A. Albanese	CSP 4-57, Syracuse, NY 13221
1	R. J. Anderson	CSP 3-35, Syracuse, NY 13221
1	C. Arabadjis	CSP 3-16, Syracuse, NY 13221
1	R. L. Benfey	CSP 5-C4, Syracuse, NY 13221
1	C. E. Blom	CSP 5-M8, Syracuse, NY 13221
1	W. C. Bookheimer	FRP 1-6D, Syracuse, NY 13221
1	R. W. Bush	CSP 3-11, Syracuse, NY 13221
1	M. M. Clark	CSP 5-J2, Syracuse, NY 13221
1	K. B. Cross	CSP 3-11, Syracuse, NY 13221
2	B. A. Deresh	CSP 5-C4, Syracuse, NY 13221
1	R. J. Drexler	CSP 5-2J, Syracuse, NY 13221
1	W. I. Fenster	CSP 5-2J, Syracuse, NY 13221
1	M. M. Fitelson	FRP 1-10B, Syracuse, NY 13221
1	M. I. Fox	FRP 1-1D, Syracuse, NY 13221
1	E. J. Gersten	CSP 5-K4, Syracuse, NY 13221
1	E. H. Gibbons	CSP 1-8, Syracuse, NY 13221
1	J. J. Gostin	CSP 3-50, Syracuse, NY 13221
1	W. D. Haynes	CSP 5-2J, Syracuse, NY 13221
1	J. F. Jaeger	FRP 1-6C, Syracuse, NY 13221
1	J. K. Jamison	CSP 4-57, Syracuse, NY 13221
1	H. L. Johndrow	CSP 5-G7, Syracuse, NY 13221
1	J. F. Jones	CSP 3-11, Syracuse, NY 13221

Copies	Name	Location
1	R. A. Loomis	CSP 5-J2, Syracuse, NY 13221
1	J. S. Mac Blane	CSP 5-J2, Syracuse, NY 13221
1	T. A. Matsumoto	CSP 1-20, Syracuse, NY 13221
1	C. A. Miglierina	CSP 3-35, Syracuse, NY 13221
1	G. H. Millman	CSP 5-4B, Syracuse, NY 13221
1	A. E. Morris	CSP 5-2J, Syracuse, NY 13221
1	D. J. Morrow	CSP 5-K7, Syracuse, NY 13221
1	K. A. Olsen	CSP 4-41, Syracuse, NY 13221
1	J. L. Perry	CSP 5-K7, Syracuse, NY 13221
1	J. E. Phillips	CSP 5-W7, Syracuse, NY 13221
1	P. E. Postell	CSP 5-K7, Syracuse, NY 13221
1	E. L. Post	CSP 5-7G, Syracuse, NY 13221
1	W. D. Putman	CSP 5-5P, Syracuse, NY 13221
1	D. T. Rakoske	CSP 5-2J, Syracuse, NY 13221
1	J. G. Reddeck	CSP 4-5, Syracuse, NY 13221
1	G. V. Richards	CSP 5-K7, Syracuse, NY 13221
1	E. B. Rockwood	CSP 5-2J, Syracuse, NY 13221
1	R. A. Schirmer	CSP 3-11, Syracuse, NY 13221
1	F. Schlect	CSP 5-G7, Syracuse, NY 13221
1	E. J. Schroeder	CSP 5-K7, Syracuse, NY 13221
1	T. B. Shields	CSP 5-K7, Syracuse, NY 13221
1	F. V. Teillon	FRP 2-14R, Syracuse, NY 13221
1	R. K. Urquhart	CSP 3-35, Syracuse, NY 13221
1	R. Wasiewicz	CSP 4-5, Syracuse, NY 13221
1	R. E. Wengert	CSP 1-20, Syracuse, NY 13221
1	R. L. Winje	FRP 1-6D, Syracuse, NY 13221
1	A. E. Zebrowski	CSP 5-K7, Syracuse, NY 13221

TABLE OF CONTENTS

i

LIST OF ILLUSTRATIONS

LIST OF ILLUSTRATIONS (CONT)

SECTION I

INTRODUCTION

Estimation of the root-mean-square (rms) target position accuracy of a radar system is of great importance to both radar manufacturers and customers. To determine whether a system meets specifications, tests are performed on real targets and position error is estimated from data which is stochastic in nature, and reflects aircraft deviations from the expected flight path as well as from sources of error within the radar itself.

For a 3-D radar, one would like to estimate the rms error in each of three coordinates: range, height, and azimuth. Three major components contribute to this error in each case. The first of these is bias, which is usually highly correlated from sample to sample, but has an error component which is random over the long run in addition to a fixed component. This error can only be characterized with reference to some external standard. The second and third components of error are jitter and thermal noise. These are both random errors which are uncorrelated from sample to sample. Their combined contribution can, in principle, be characterized without need for an external standard. The jitter component is due to a variety of independent random sources and can usually be treated accurately as Gaussian and independent of target range. The contribution of range-dependent thermal noise is also Gaussian, and because the coordinate estimation processes are only weakly nonlinear, the sum of these effects is still effectively Gaussian. It is the variance of these random components that we wish to estimate as zero mean processes, thus requiring a separation of the mean flight path from the measurement errors.

The traditional procedures for determining positional accuracy consist of a series of controlled flights. These generally involve an aircraft flying an approximately radial flight path (with respect to the radar) at a constant altitude. The intent here is to control the target radar cross section (RCS) and to permit simplified flight path models. Usually two or more legs are run (e.g. inbound and outbound) at each of several altitudes. Quite often little or no thought is given to the quality of the measured and estimated quantities in terms of the effect of limited sample sizes on estimation error. Both the producer and the buyer thus suffer unknown risks of the radar falsely failing the test or falsely passing, respectively.

The total rms error (bias and random) of the radar under test can be estimated by reference to the simultaneous track of a precision tracking radar with known errors which are significantly less than the radar under test. Alternatively the error can be separated into two parts, with bias error determined through static tests or other means and the random error estimated from least squares fits of the tracking data to some simple trend model (e.g., zeroth-order in height and azimuth and linear in range for a radial flight path).

Several practical problems are immediately evident when analyzing data from flight tests. First, if the tests are manually conducted using an operator-controlled track ball/ target window on the plan position indicator (PPI) for instance, operator error can be a significant contribution to the total error. This is especially true near the limits of coverage and detection, in the vicinity of crossing aircraft, and in regions of clutter leak through. Second, deviations from a true radial flight path, including offsets and perturbations as from gusts, can cause severe nonlinearities with equivalent polynomial orders of fit as high as ten or more, particularly when the target is near the radar. Because of these reasons, simple a priori models can lead to position errors many times larger than the contribution from the radar system alone.

Often the radar will be tested in a location which precludes the availability of a separate reference radar and the second approach is the only practical alternative. Accordingly, this paper addresses the problem of estimating the variance of the random error component without a precision reference standard, providing a systematic, rigorous approach which is unbiased in the mean and independent of the true aircraft flight path.

The method is quite general to sensors and targets of all types even though the specific application it was developed for was a radar under test with an aircraft on a radial path.

The statistics of the estimate are known and the concept of risk can be used to effectively design the test (e.g., number of legs) in the first place, while the concept of confidence bounds can be used to effectively evaluate the test results afterwards.

Figures 1-1 and 1-2 are PPI plots of actual radar data taken from a modern tactical radar. They illustrate some of the difficulties involved in flying easily modelled paths. The target in Figure 1-1 is a Lear jet attempting to fly radial flight paths. The actual paths being flown are not even linear in cartesian space, much less in the space defined by the coordinates of range (R), height (H), and azimuth (A). Because of this, a linear

1-2
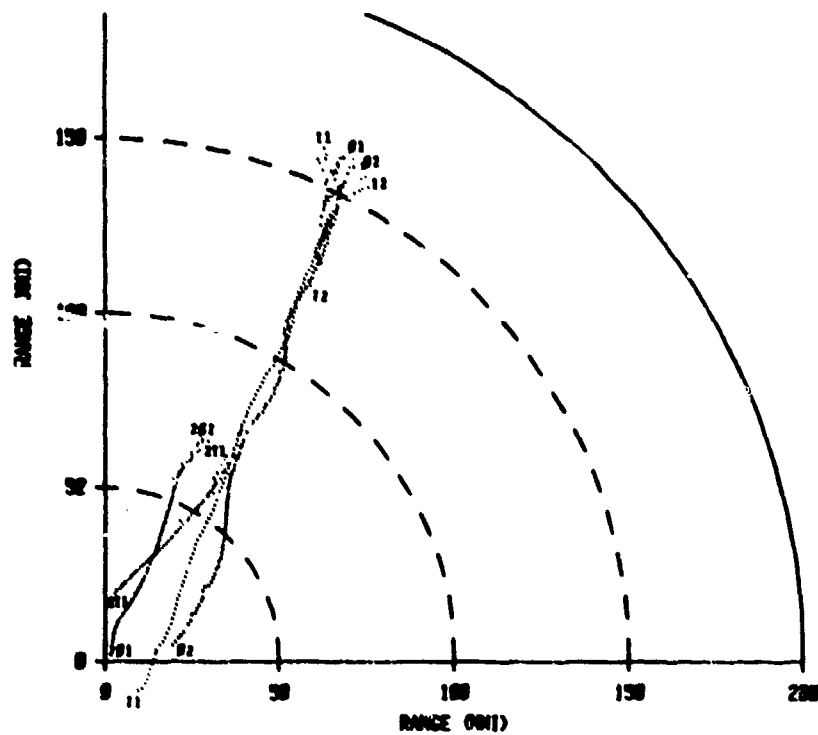
Figure 1-1. Actual PPI Tracks of Lear Jet Legs
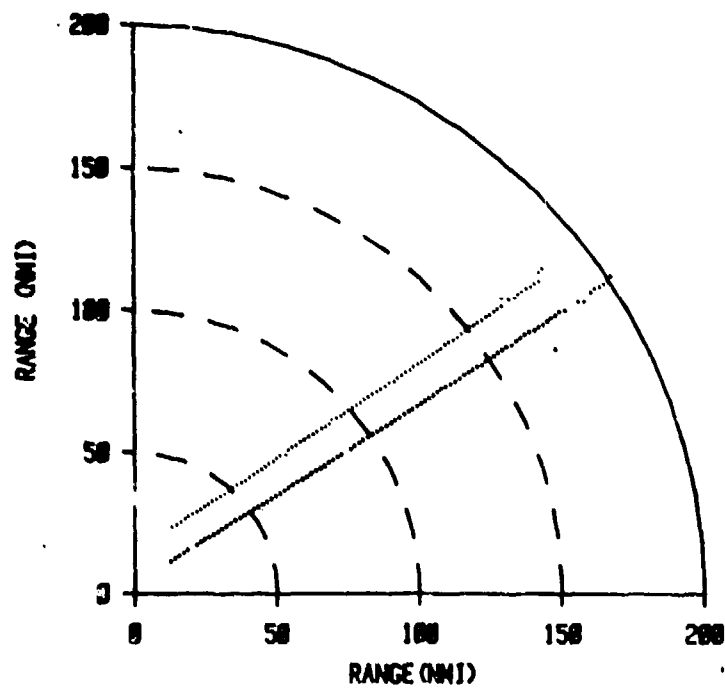
Figure 1-2. PPI For Fighter at 38 kft Nominal

1-3

model is severely inadequate as a trend mode. The target in Figure 1-2 is a military fighter plane, also attempting to fly radial flight paths. Here, the path is very close to being linear in cartesian space, but is still very nonlinear in radar space particularly at close range. Again, if simple flight path models are used, they will give rise to severe estimation errors.

As evidence of this thesis, Figure 1-3 shows the estimated error in azimuth as a function of range for one of the flights in Figure 1-2. The dotted line in this figure represents the theoretical standard deviation of the random error as predicted by theoretical models of the radar. These models include the effects of stepped (clutter-rejection) attenuators which cause the discontinuities in the curve. The dashed line is the one-sigma random error calculated from the flight data after removal of the mean. This corresponds to an assumed radial flight path. The solid line shows the one-sigma random error calculated from the flight data after the removal of an assumed linear (in azimuth) trend. The broken
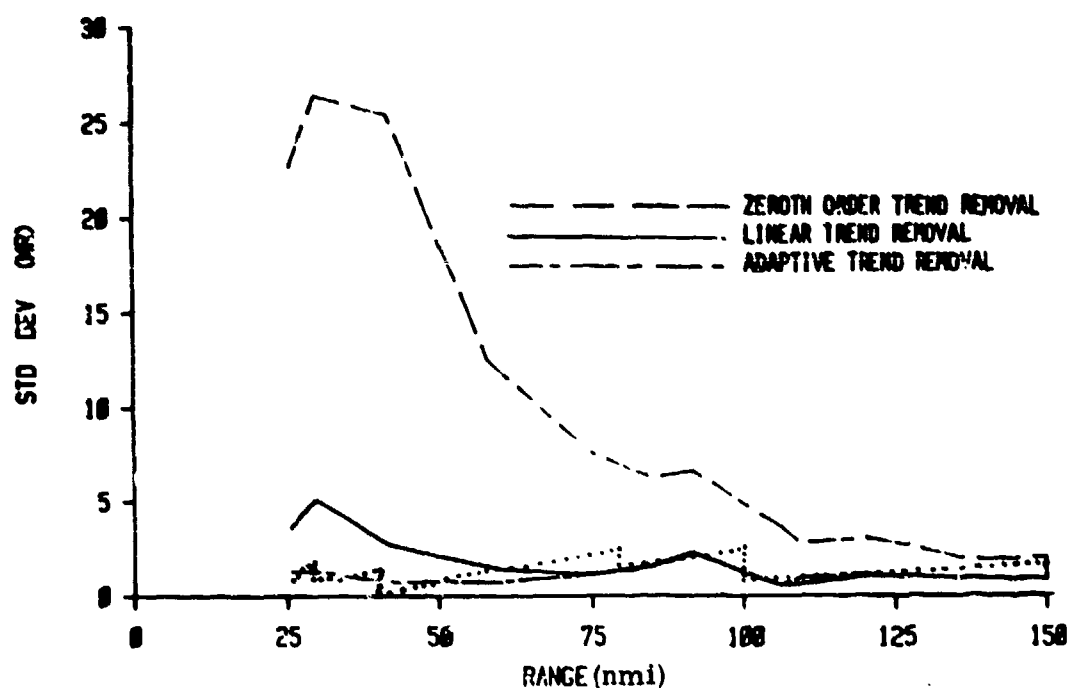
Figure 1-3. Rms Azimuth Accuracy for Fighter at 38 kft

line shows the one-sigma random error calculated by the method proposed in this paper, where the order of the assumed trend is determined from the data itself. Notice that the constant azimuth assumption leads to severe overestimation and even the assumption

1-4

of a linear trend produces relatively large estimation errors. The error estimate calcu-
lated by the proposed method, however, shows good correlation with the predicted value.

Figure 1-4 shows a plot of the one-sigma random error in range, as a function of
range, for a fighter at 17,000 ft. As before, error calculations based on a linear trend
appear as a solid line, calculations based on the proposed method as a broken line, and
predicted theoretical error as a dotted line. Notice again how poorly the linear trend
assumption compares with the proposed model.

These figures illustrate the need for a method of variance estimation which
isolates the random errors in the system from the mean flight path. The method developed
here addresses this problem directly and, in doing so, overcomes many of the pitfalls of
the simpler methods.
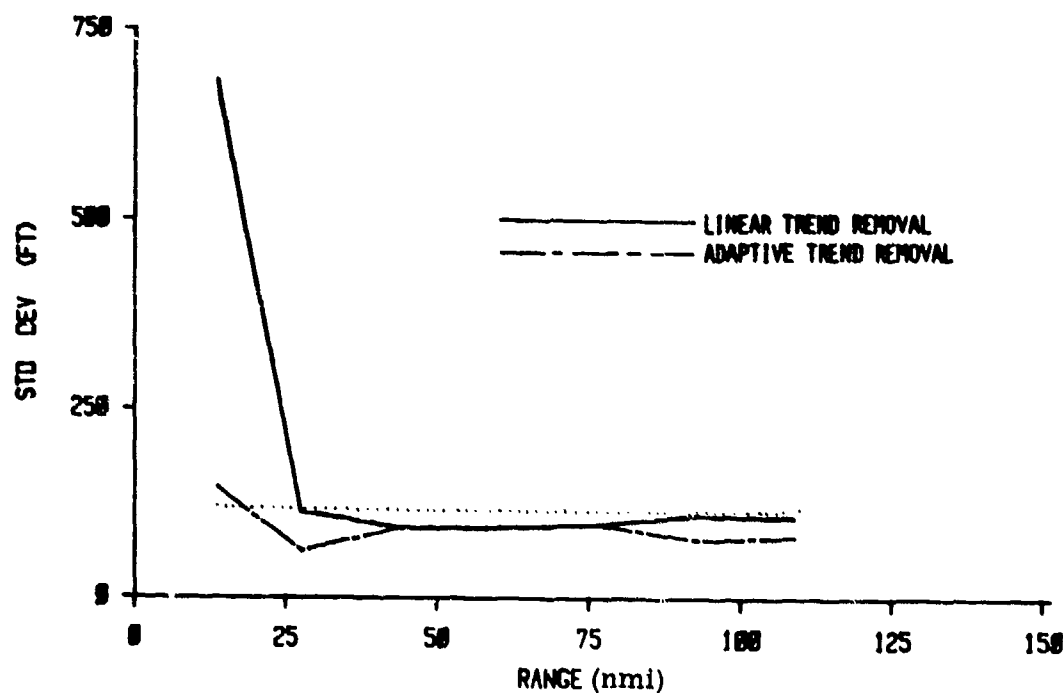
Figure 1-4. Rms Range Accuracy for Fighter at 17 kft

1.1 SUMMARY

Because the random components of error in all three coordinates (R, H, and A) are closely represented by zero-mean Gaussian processes, it is assumed that the analysis below can be applied with equal validity to any of these parameters. For this reason, the analysis has been carried out in terms of the general coordinate Z, which can be either R, H, or A. It will be shown that the variance of the random components of error, σ^2, can be estimated from incomplete data (data points missing), using a polynominal trend model. This estimate is unbiased and independent of the trend removal process in the mean. The trend removal process is adaptive, statistically sound, rigorous, and independent of a priori or external data. It will be shown that overfitting the trend gives the same estimate of the variance in the mean as optimal fitting. It will also be shown that the adjacent point correlation coefficient can be used as an indication of overfitting, thereby insuring proper fit.

After developing the variance estimation procedure, the statistics of the estimation error will be derived and shown to be directly relatable to the way in which the test is carried out. Then the producer's risk of the radar falsely failing the test and the buyer's risk of the radar falsely passing the test will be derived as a function of the statistical uncertainty created by limited sample sizes. These are important features of a well designed acceptance test in which both types of statistical risks are quantified and constrained to mutually agreed levels. Additionally expressions are developed and algorithms presented for estimating confidence bounds on the true variance given the actual estimate.

In all cases, simulation has been used to confirm theoretical techniques in the face of real-world applications. Also shown are the results of a comparison of this technique with the use of an external standard of reference in conjunction with data collected during actual flight tests.

SECTION II

UNBIASED OPTIMAL ESTIMATION OF VARIANCE

2.1 DERIVING THE UNBIASED FORM FOR KNOWN POLYNOMINAL ORDER K

As a starting point, assume that the actual polynominal trend of the mean target flight path is of known order, K, with additive independent samples of Gaussian noise. Taking N measured data points, denote

$$\underline{Z} = [Z_1 \, Z_2 \dots Z_N]^T = \underline{P} \, \underline{b} + \underline{v} \tag{2-1}$$

as the set of measured positions, e.g., range, azimuth, or height, in a specified time or range interval, where

$$\underline{v} = [v_1 v_2 \dots v_n]^T \tag{2-2}$$

is the set of independent noise samples with

$$E(v_j) = 0 \quad \text{and} \quad E(v_i v_j) = \sigma^2 \delta_{ij} . \tag{2-3}$$

The jth point of the true mean flight path is

$$\bar{Z}_j = \sum_{i=1}^{K+1} b_i P_{ji} \tag{2-4}$$

where the P_{ji} are polynominals with $j \in N$ and $i \in K+1$. The vector of true coefficients is

$$\underline{b} = \left[b_1 b_2 \dots b_{K+1} \right]^T$$

and the polynominal matrix is

$$\underset{(N \times K+1)}{\underline{P}} = \begin{bmatrix} P_{11} P_{12} \dots \dots P_{1,K+1} \\ \vdots \quad \cdot \quad \cdot \quad \vdots \\ \vdots \quad \quad \cdot \quad \cdot \quad \vdots \\ \vdots \quad \quad \quad \cdot \quad \vdots \\ P_{N1} \dots \dots \dots P_{N,K+1} \end{bmatrix} \tag{2-6}$$

If a polynominal of order K is assumed (it doesn't matter whether it is the same polynominal so long as it is complete over the same space), then the assumed trend is (2-5)

$$\underline{\hat{z}} = \underline{P}\,\underline{\hat{b}} \tag{2-7}$$

where by the method of least squares,

$$\underline{\hat{b}} = \left[\hat{b}_1\, \hat{b}_2 \ldots \hat{b}_{K+1} \right]^T = (\underline{P}^T \underline{P})^{-1}\, \underline{P}^T \underline{z}\,. \tag{2-8}$$

Defining the set of residuals

$$\underline{\tilde{z}} \triangleq \underline{z} - \underline{\hat{z}} \tag{2-9}$$

and ignoring a weighting matrix for simplicity, the maximum likelihood estimate of the variance σ^2 is

$$\sigma^2_{ML} = \frac{1}{N}\, \underline{\tilde{z}}^T \underline{\tilde{z}}\,. \tag{2-10}$$

In order to examine the structure of the estimate, first introduce Equations (2-1), (2-7), and (2-8) into the expression for the residual, i.e., Equation (2-9). Thus

$$\underline{\tilde{z}} = (\underline{I} - \underline{M})\underline{v}, \tag{2-11}$$

where $\underline{I}$ is the identity matrix and

$$\underline{M} \triangleq \underline{P}(\underline{P}^T \underline{P})^{-1}\underline{P}^T. \tag{2-12}$$

Note that the expected value of $\underline{\tilde{z}}$ is zero so that the residuals themselves are unbiased. Introducing equations (2-11) and (2-12) into (2-10), recognizing that $\underline{M}$ is idempotent (i.e., $\underline{M}^2 = M$) and symmetric (i.e., $\underline{M}^T = M$) then

$$\widehat{\sigma^2}_{ML} = \frac{1}{N}\, \underline{v}^T (\underline{I} - \underline{M})\underline{v}\,. \tag{2-13}$$

Because this is in quadratic form and the noise samples are uncorrelated, the expectation value is

$$E\,\widehat{\sigma^2}_{ML} = \frac{\sigma^2}{N}\, \text{Trace}\,(\underline{I} - \underline{M})\,. \tag{2-14}$$

Note that the dimensions of $\underline{I}$ are NxN and that

$$\text{Trace } (\underline{I}-\underline{M}) = N - \text{Trace } \underline{P} \, (\underline{P}^T \underline{P})^{-1} \underline{P}^T$$

$$= N - \text{Trace } (\underline{P}^T \underline{P})^{-1} \underline{P}^T \underline{P} = N - (K+1)$$

because the dimensions of $\underline{P}$ are NxK+1. Thus

$$E \, (\hat{\sigma}^2_{ML}) = \sigma^2 (\frac{N-K-1}{N}) \qquad (2\text{-}15)$$

which is biased low for all $K \geq 0$. An unbiased estimate of variance can be constructed however from

$$\hat{\sigma}^2 \cong \frac{\tilde{\underline{Z}}^T \tilde{\underline{Z}}}{N-(K+1)} , \qquad (2\text{-}16)$$

where

$$E \, (\hat{\sigma}^2) = \sigma^2 \qquad (2\text{-}17)$$

for all $N > K+1$.

This formulation reflects the equivalent loss of data points in the estimation of the K+1 polynominal coefficients from the same data for which the variance is estimated. The reader will note the familiar form this reduces to when K = 0, i.e.,

$$\hat{\sigma}^2 = \frac{\sum_{i=1}^{N} (Z_i - \bar{Z}_i)^2}{N-1} \qquad (2\text{-}18)$$

for which the mean trend is just the average value of the data

$$\bar{Z} = \frac{1}{N} \sum_{i=1}^{N} Z_i . \qquad (2\text{-}19)$$

SECTION III

SUBOPTIMAL ESTIMATION OF VARIANCE

In general, the true order of the mean flight path, K, is unknown. Computationally, an order, M, is assumed which may be less than (underfitting) or greater than (overfitting) the true order K.

3.1 UNDERFITTING WITH ORDER M<K

Intuitively, it is clear that underfitting is dangerous because actual deviations of the true flight path from the assumed flight path will show up as a bias in the variance estimate. To see this analytically, consider the estimation of the $M+1$ polynominal coefficients and the resulting residuals. Thus, we partition all matrices at the boundary of estimatable quantities such that

$$\underset{(NxM+1)}{\underline{P}} \equiv \left[\underset{(NxM+1)}{\underline{P_1}} \; \middle| \; \underset{(NxK-M)}{\underline{P_2}} \right] = \begin{bmatrix} P_{11} \cdots \cdots P_{1,M+1} & P_{1,M+2} \cdots P_{1,K+1} \\ \vdots & \vdots & \vdots & \vdots \\ \vdots & \vdots & \vdots & \vdots \\ \vdots & \vdots & \vdots & \vdots \\ P_{N1} \cdots \cdots P_{N,M+1} & P_{N,M+2} \cdots P_{N,K+1} \end{bmatrix} \tag{3-1}$$

and

$$\underline{\hat{b}} = \left[\underline{\hat{b}_1}^T \; \middle| \; \underline{\hat{b}_2}^T \right]^T = \left[\hat{b}_1 \hat{b}_2 \cdots \hat{b}_{M+1} \; \middle| \; \hat{b}_{M+2} \cdots \hat{b}_{K+1} \right]^T \tag{3-2}$$

where

$$\underline{\hat{b}_1} = (\underline{P_1}^T \underline{P_1})^{-1} \underline{P_1}^T \underline{Z} \tag{3-3}$$

and

$$\underline{\hat{b}_2} = 0. \tag{3-4}$$

Defining a new matrix

$$\underline{M_1} \triangleq \underline{P_1} (\underline{P_1}^T \underline{P_1})^{-1} P_1^T \tag{3-5}$$

then

$$\hat{\underset{\sim}{Z}} = \underline{P}\ \underline{b} + \underline{v} - \underline{P}_1\ \hat{\underline{b}}_1 = (\underline{I} - \underline{M}_1)(\underline{P}_2\ \underline{b}_2 + \underline{v}) \tag{3-6}$$

and

$$E(\hat{\underset{\sim}{Z}}) = (\underline{I} - \underline{M}_1)\ \underline{P}_2\ \underline{b}_2 \neq 0. \tag{3-7}$$

Thus the residuals have an incorrectable bias error because of the unknown true coefficients $\underline{b}_2 \neq 0$. Moreover, after substituting into Equation (2-10) for the traditional variance estimate

$$\hat{\hat{\sigma}}_{ML}^2 = \sigma^2\left(\frac{(N-M+1)}{N}\right)$$
$$+ \frac{1}{N}\sum_{j=1}^{N}\left\{\left(\sum_{j=M+2}^{K+1} b_i P_{ij}\right)^2\left(1 - M_{1_{jj}}\right)\right. \tag{3-8}$$
$$\left. -2\sum_{\ell=j+1}^{N} M_{1_{j\ell}}\sum_{i=M+2}^{K+1} b_i P_{ij}\sum_{i=M+2}^{K+1} b_i P_{i\ell}\right\}$$

it is clear that while the first term is of the form which has a correctable bias, the remainder is hopelessly structured with the unknown and arbitrary true polynominal coefficients $\underline{b}_2$. Thus, underfitting causes uncontrollable and arbitrarily large bias errors which explain the large errors seen in Figures 1-3 and 1-4*. Clearly under-fitting is to be avoided at all costs.

---

*While it has not yet been proved in general, simulation supports the notion that underfitting leads invariably to overestimation. As an example, consider the simplest case where K=1 and M=0. Using the unbiased expression for variance, i.e., Equation (2-16), replacing K by M and equally spaced data points Δt seconds apart then

$$E(\hat{\sigma}^2) = \sigma^2 + \frac{N(N-1)\ (N+1)}{12}\ b_2^2\ \Delta t^2$$

such that

$$E(\hat{\sigma}^2) > \sigma^2 \text{ for all } N > 1.$$

3.2   OVERFITTING WITH ORDER M > K

Intuitively, overfitting appears dangerous because the polynominal fit to the trend may fit the noise we wish to characterize. Surprisingly, this fear is not justified. Consider a new partitioning at the boundary of true quantities such that

$$\underset{(N \times M+1)}{\underline{P}} = \left[\begin{array}{c|c} \underline{P}_1 & \underline{P}_2 \end{array} \right] = \left[\begin{array}{ccc|ccc} P_{11} & \cdots\cdots & P_{1,\,K+1} & P_{1,\,K+2} & \cdots & P_{1,\,M+1} \\ \vdots & & \vdots & & & \\ \vdots & & \vdots & & & \\ \vdots & & \vdots & & & \\ P_{N1} & \cdots\cdots & P_{N,\,K+1} & P_{N,\,K+2} & \cdots & P_{N,\,M+1} \end{array} \right] \qquad (3\text{-}9)$$

$$\underset{(N \times K+1)\,(N \times M-K)}{}$$

and

$$\hat{\hat{\underline{b}}} = \left[\begin{array}{c|c} \hat{\hat{\underline{b}}}_1 & \hat{\hat{\underline{b}}}_2 {}^T \end{array} \right]^T = \left[\begin{array}{cccc|ccc} \hat{\hat{b}}_1 & \hat{\hat{b}}_2 & \cdots & \hat{b}_{K+1} & \hat{b}_{K+2} & \cdots & \hat{b}_{M+1} \end{array} \right]^T \qquad (3\text{-}10)$$

where

$$\hat{\hat{\underline{b}}} = \left(\underline{P}^T \underline{P} \right)^{-1} \underline{P}^T \underline{Z} \qquad (3\text{-}11)$$

and

$$\hat{\hat{\underline{Z}}} = \underline{P}_1 \underline{b}_1 + \underline{v} - \underline{P}\,\hat{\hat{\underline{b}}} \; . \qquad (3\text{-}12)$$

Substituting Equation (3-11) into (3-12) and simplifying

$$\hat{\hat{\underline{Z}}} = (\underline{I}\text{-}\underline{M})\ \underline{Z} = (\underline{I}\text{-}\underline{M})\ \underline{P}_1\,\underline{b}_1 + (\underline{I}\text{-}\underline{M})\,\underline{v}, \qquad (3\text{-}13)$$

which is the same as Equation (2-11) for the case of M-K except for the first term. But since

$$(\underline{I}\text{-}\underline{M})\ \underline{P} = 0 \qquad (3\text{-}14)$$

all partitions of $(\underline{I}-\underline{M})$ $\underline{P}$ must be zero as well. Thus

$$(\underline{I}-\underline{M})\,\underline{P}_1\,\underline{b}_1 = 0 \qquad\qquad (3\text{-}15)$$

and

$$\hat{\underline{Z}} = (\underline{I}-\underline{M})\,\underline{v}, \qquad\qquad (3\text{-}16)$$

which is exactly the same result achieved for the optimal case where the polynomial order is known beforehand. Thus overfitting leads to unbiased residuals and an unbiased estimate of variance can be constructed from

$$\hat{\hat{\sigma}}^2 \triangleq \frac{\hat{\underline{Z}}^T\hat{\underline{Z}}}{N-(M+1)} \qquad\qquad (3\text{-}17)$$

with

$$\hat{\underline{Z}} = (\underline{I}-\underline{M})\,\underline{Z} \qquad\qquad (3\text{-}18)$$

where the hat implies suboptimization in the sense that K is not known but $M \geq K$ is somehow guaranteed (i.e., overfitting).

The surprising result of this analysis is that an unbiased optimal estimate of variance can be achieved, i.e.,

$$E\left(\hat{\hat{\sigma}}\right) = \sigma^2 \qquad\qquad (3\text{-}19)$$

for all

$$K \leq M < N\text{-}1. \qquad\qquad (3\text{-}20)$$

Intuitively, it seems as though overfitting merely fits the noise. If $M = N\text{-}1$ then this notion is correct. However, so long as $M \leq N\text{-}2$ the trend does not quite fit the noise (although it is influenced by it), and the variance estimation formula, i.e. Equation (3-17) exactly scales the residuals in the mean to their correct value just as if $M = K$.

Figures 3-1 and 3-2 illustrate this. The dashed curve in Figure 3-1 shows simulated noise as fit by the curve when $M = N-1$ and $K = 0$. The solid curve represents an overfit where $M = N-2$. Note that while influenced by the noise, there are still finite residuals as shown in Figure 3-2. These residuals are exactly scaled in the mean to their optimal value, i.e. $M = K$, by the factor $\sqrt{N/(N-M-1)}$.
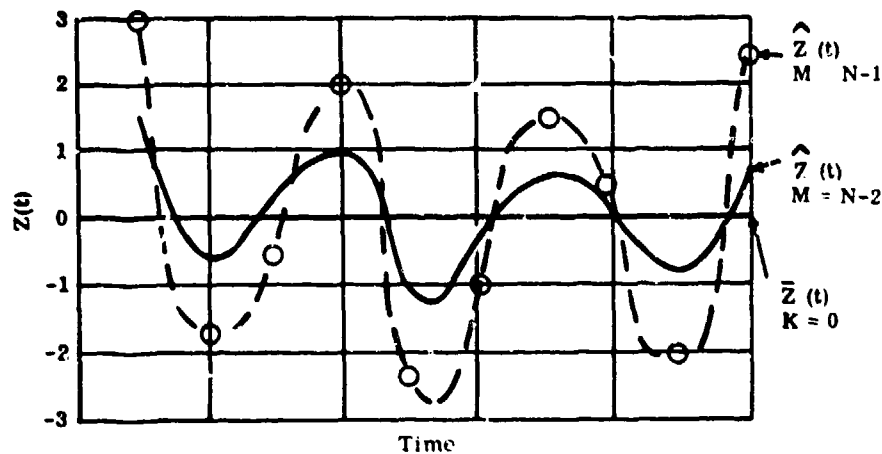
Figure 3-1. Measured Data (Gaussian Noise Plus Zeroth Order Trend)
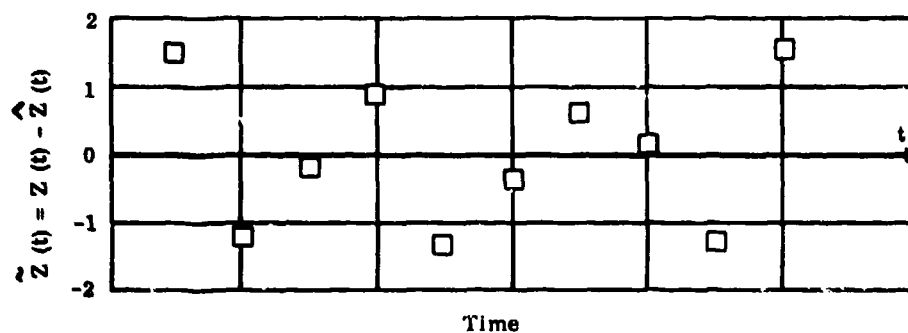
Figure 3-2. Residuals for $M = N-2$

To fix ideas about the variance estimate, consider Figure 3-3 which shows the effect of residual scaling for $N = 10$, $K = 0$, $\sigma = 1$ as a function of M, the assumed order. The lower curve on the left shows the standard deviation (root variance estimate) without scaling. Here is the support for our intuition of decreasing variance until $M = N-1$ where the noise is exactly fit. The upper curve on the left shows that the bias correction factor $\sqrt{N/(N-M-1)}$ exactly scales the residuals for all $M < N-1$.
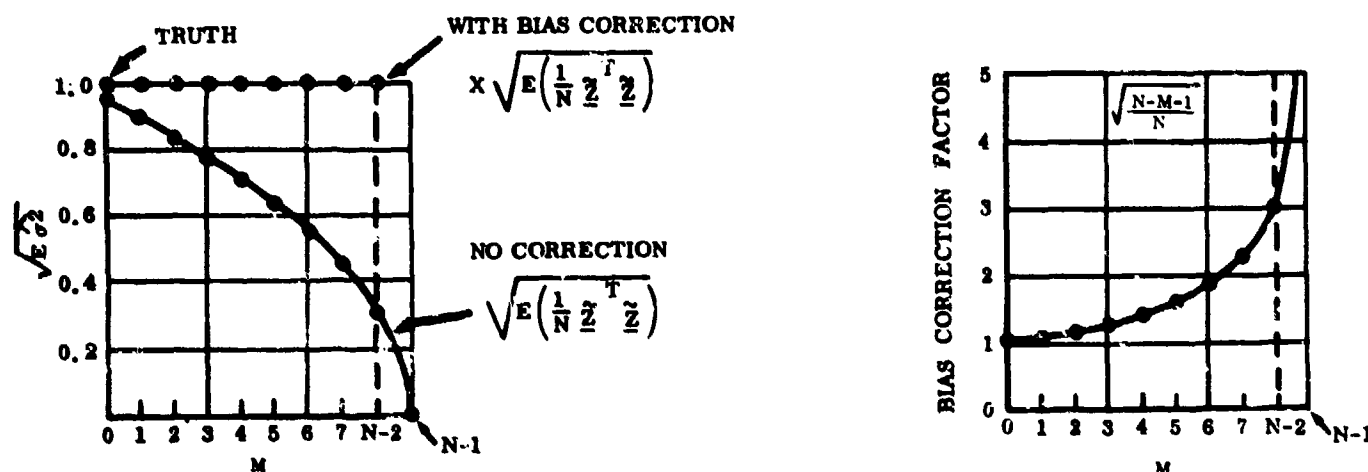
Figure 3-3. Numerical Example of Variance Estimates with Overfitting ($N = 10$, $K = 0$)

The plot on the right shows the variation of the bias correction factor as a function of M (for $K=0$). Here it can be seen that this correction factor which scales the residuals must increase as M is increased over K until at $M=N-1$ this factor must be unrealizably infinite for the correspondingly zero residuals. The message here is that so long as $K \leq M \leq N-2$ the correction factor works and unbiased estimates of variance will result.

SECTION IV

ADJACENT POINT AUTOCORRELATION AS AN INDICATOR OF OVERFITTING

It was shown, on the one hand, that underfitting leads to uncorrectable bias errors while overfitting, on the other hand, will always yield an unbiased estimate so long as

$$N-1 > M \geq K. \tag{4-1}$$

This result is only useful when accompanied by a reliable method for ensuring that $M \geq K$. As it happens, a sensitive indicator of overfitting is the adjacent point correlation coefficient defined by

$$\hat{\rho} \triangleq \frac{1}{\sigma^2} \left[\frac{\tilde{Z}^T \underline{U} \tilde{Z}}{N - (M+1)} \right] \tag{4-2}$$

where all definitions are as before except for the lag matrix defined by

$$\underset{(N \times N)}{\underline{U}} \triangleq \begin{bmatrix} 0 & 1 & 0 & \ldots & \ldots & 0 \\ 0 & 0 & 1 & & & \vdots \\ \vdots & & & \ddots & & \vdots \\ \vdots & & & & \cdot 1 & 0 & 0 \\ \vdots & & & & & 1 & 0 \\ \vdots & & & & & 0 & 1 \\ 0 & \ldots & \ldots & \ldots & 0 & 0 \end{bmatrix} \tag{4-3}$$

4.1 CONCEPT

Underfitting results in residuals which are positively correlated because adjacent pairs are mostly of the same sign. This effect is illustrated in Figure 4-1. Moreover, the greater the underfit, the more positive the correlation. Overfitting, on the other hand, results in residuals which are negatively correlated because adjacent pairs are mostly of opposite sign. This effect is illustrated in Figure 4-2. The greater the overfit, the more negative the correlation. Only in the limit of $M = N-1$ does the correlation coefficient reach -1.

Thus, one can expect that the mean value of $\hat{\rho}$ will become negative when M just exceeds K. Of course, it isn't really necessary to determine this point precisely because the variance estimate will still be unbiased no matter how much M exceeds K (except for $M = N-1$). This provides a cushion to protect against the fluctuations in the estimate of $\hat{\rho}$.
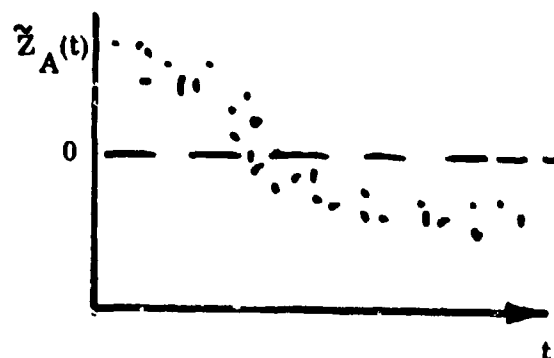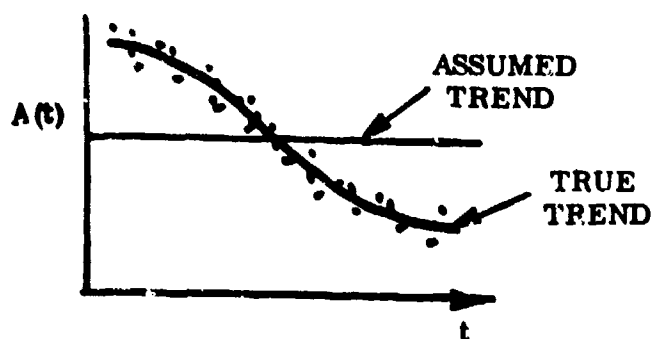
Figure 4-1. Measured Data and Residuals with an Underfit Trend
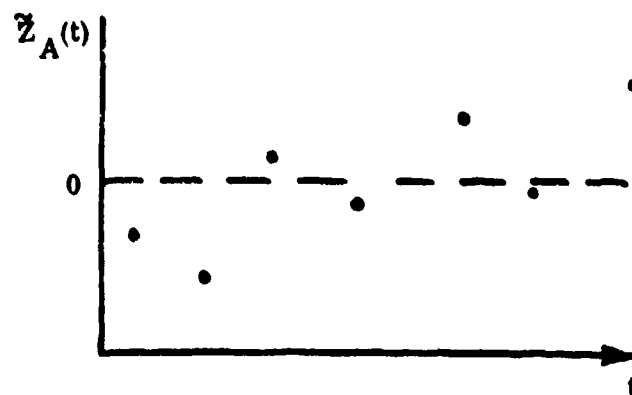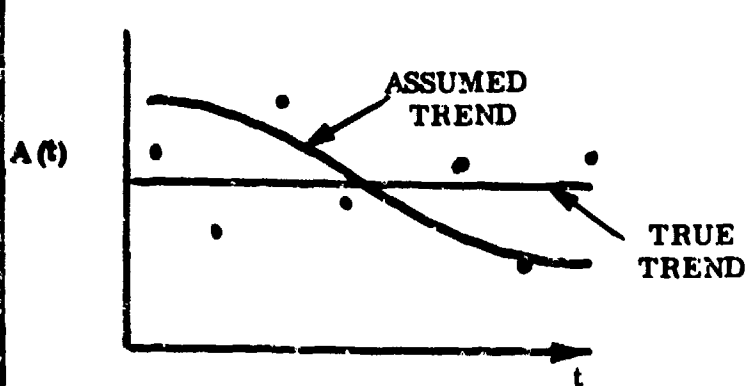
Figure 4-2. Measured Data and Residuals with an Overfit Trend

4.2 ANALYSIS

The expectation value of $\hat{\rho}$ from Equations (3-18) and (4-2) when $M \geq K$ is,

$$E(\hat{\rho}) = \frac{1}{N-(M+1)} \text{ Trace } \left[(\underline{I}-\underline{M})^T \underline{U} (\underline{I}-\underline{M})\right] = -\frac{\text{Trace } (\underline{U} \, \underline{M})}{N-(M+1)}. \qquad (4-4)$$

where we note that Trace $\underline{U} = 0$ and $(\underline{I}-\underline{M})$ is idempotent. From the definition of $\underline{M}$,

$$\text{Trace}(\underline{U} \, \underline{M}) = \text{Trace}\left(\underline{P}^T \underline{P}\right)^{-1} \underline{U} \, \underline{P} \, \underline{P}^T . \qquad (4-5)$$

If $\underline{P}$ is a complete set of orthogonal polynomials over domain N then

$$\sum_{j=1}^{N} P_{j\ell} \, P_{jk} \left\{ \begin{array}{l} 0; \ell \neq k \\[2mm] \sum_{j=1}^{N} P_{jk}^2 ; \ell = k \end{array} \right. \qquad (4-6)$$

and $\underline{P}^T \underline{P}$ is diagonal. Thus,

$$\text{Trace}(\underline{U} \, \underline{M}) = \sum_{k=1}^{K+1} \left\{ \frac{P_{1k} P_{2k} + \cdots\cdots + P_{N-1,\,k} P_{Nk}}{\displaystyle\sum_{j=1}^{N} P_{jk}^2} \right\} \qquad (4-7)$$

and

$$E(\hat{\rho}) = -\frac{1}{N-M-1} \sum_{k=1}^{K+1} \left\{ \frac{\displaystyle\sum_{j=1}^{N-1} P_{jk} P_{j+1,\,k}}{\displaystyle\sum_{j=1}^{N} P_{jk}^2} \right\} . \qquad (4-8)$$

Without formal proof, laborious analyses for $M = 0$, 1, and 2, and numerical simulations for M as high as 20 establish that

$$E(\hat{\rho}) = -\frac{M+1}{N}; \quad N-1 > M \geq K . \qquad (4-9)$$

This remarkable result is independent of the choice of polynomial, orthogonal or otherwise, so long as it is complete over the domain of N.

Of course Equation (4-2) is not a form suitable for calculation because of the need to know σ^2, the true variance, beforehand. A practical expression for this purpose which has the same expectation value, i.e., Equation (4-9), is as follows:

$$\hat{\rho} = \frac{\displaystyle\sum_{j=1}^{N-1} \left(z_j - \hat{\bar{z}}_j\right)\left(z_{j+1} - \hat{\bar{z}}_{j+1}\right)}{\left\{ \displaystyle\sum_{j=1}^{N-1} \left(z_j - \hat{\bar{z}}_j\right)^2 \sum_{j=2}^{N} \left(z_j - \hat{\bar{z}}_j\right)^2 \right\}^{1/2}} \quad . \tag{4-10}$$

4-4

SECTION V

REDUCING ESTIMATION ERROR

Because the maximum likelihood estimate is the minimum variance estimator of variance, the estimation error will be increased by the bias correction factor $N/(N-M-1)$. A practical way of reducing this error is to use a larger data set for the trend removal than for the variance estimate.

5.1 ANALYSIS

Consider the partitioning of the N data points for trend removal into three parts, the central one being used for the estimate of variance. Thus,

$$\underline{Z} = \left[\underline{Z_1}^T \mid \underline{Z_2}^T \mid \underline{Z_3}^T \right]^T = \left[Z_1 Z_2 \ldots Z_r \mid Z_{r+1} \ldots Z_s \mid Z_{s+1} \ldots Z_N \right]^T \quad (5\text{-}1)$$

and $\underline{P}$ is similarly partitioned horizontally as

$$\underset{(N \times K+1)}{\underline{P}} = \left[\underset{(r \times K+1)}{\underline{P_1}} \mid \underset{(s-r \times K+1)}{\underline{P_2}} \mid \underset{(N-s \times K+1)}{\underline{P_3}} \right]^T \quad (5\text{-}2)$$

Then

$$\hat{\sigma}^2_{ML} = \frac{1}{s-r} \tilde{\underline{Z}}_2^T \tilde{\underline{Z}}_2 = \frac{1}{s-r} \underline{v}^T \left[\underline{I} - \underline{M} \right]_2^T \left[\underline{I} - \underline{M} \right]_2 \underline{v}. \quad (5\text{-}3)$$

Denoting

$$\underline{v}_{22} = \left[\underline{I} - \underline{M} \right]_2^T \left[\underline{I} - \underline{M} \right]_2 \quad (5\text{-}4)$$

with the $\underline{I} - \underline{M}$ matrix partitioned

$$\underline{I} - \underline{M} = \begin{bmatrix} \underline{I} - \underline{M}_{11} & \vdots & -\underline{M}_{12} & \vdots & -\underline{M}_{13} \\ - - - - - & \vdots & - - - - - & \vdots & - - - - - \\ -\underline{M}_{21} & \vdots & \underline{I} - \underline{M}_{22} & \vdots & -\underline{M}_{23} \\ - - - - - & \vdots & - - - - - & \vdots & - - - - - \\ -\underline{M}_{31} & \vdots & -\underline{M}_{32} & \vdots & \underline{I} - \underline{M}_{33} \end{bmatrix} \tag{5-5}$$

then

$$\underline{\nu}_{22} = \begin{bmatrix} -\underline{M}_{21}{}^T \\ - - - \\ \underline{I} - \underline{M}_{22} \\ - - - \\ -\underline{M}_{23}{}^T \end{bmatrix} \times \begin{bmatrix} -\underline{M}_{21} & \vdots & \underline{I} - \underline{M}_{22} & \vdots & -\underline{M}_{23} \end{bmatrix} . \tag{5-6}$$

Because Equation (5-3) is in the quadratic form

$$\widehat{\sigma}^2_{ML} = \frac{1}{s-r} \, \underline{v}^T \, \underline{\nu}_{22} \, \underline{v} \tag{5-6A}$$

then

$$\widehat{\sigma}^2_{ML} = \frac{\sigma^2}{s-r} \, \text{Trace} \, \underline{\nu}_{22} . \tag{5-6B}$$

From Appendix A where the polynomials are assumed to be orthogonal,

$$E\left(\sigma^2_{ML}\right) = \frac{\sigma^2}{s-r} \left[s-r - \sum_{k=1}^{M+1} \frac{\displaystyle\sum_{n=r+1}^{S} P^2_{nk}}{\displaystyle\sum_{n=1}^{N} P^2_{nk}} \right] \tag{5-6C}$$

so that an unbiased estimate of variance for

$$s-r \leq N$$

is,

$$\sigma^2 \triangleq \cfrac{\tilde{\underline{Z}}_2^T \, \tilde{\underline{Z}}_2}{s-r - \displaystyle\sum_{k=1}^{M+1} \cfrac{\displaystyle\sum_{n=r+1}^{S} P_{nk}^2}{\displaystyle\sum_{n=1}^{N} P_{nk}^2}} \tag{5-7}$$

which reduces to the prior result, i.e. Equation (3-17) for $s-r = N$. To see that the uncertainty in the variance estimate has been decreased by extending the domain of the fit to the trend, consider that the bias correction factor $\sigma^2 / E\!\left(\hat{\sigma}_{ML}^2\right)$ is much less for a given number of data points $s-r$. Thus if $s-r$ data points are used for the variance estimate in either case, the ratio of bias correction factors with $N > s-r$ and $N = s-r$ is,

$$\cfrac{s-r - (M+1)}{s-r - \displaystyle\sum_{k=1}^{M+1} \cfrac{\displaystyle\sum_{n=r+1}^{S} P_{nk}^2}{\displaystyle\sum_{n=1}^{N} P_{nk}^2}} < 1 \; . \tag{5-8}$$

This is so because

$$\sum_{n=r+1}^{S} P_{nk}^2 < \sum_{n=1}^{N} P_{nk}^2 \tag{5-9}$$

Figure 5-1 is a plot of this ratio for s-r=10 and N=30 for $0 \leq M \leq 9$ with K=0. Notice that for M=9, the numerator goes to zero because in the case where L=N=30, N-1=9 and all points are precisely fit. As discussed in Section III, the residuals are scaled exactly to truth in the mean for all cases where M < N-1. Thus we see here another advantage to increasing N over L in that it permits higher order fits without fitting all the points. This is offset somewhat however in that the larger N is (with a given spacing),the larger M has to be in general. Nevertheless the advantage still accrues for many cases of interest. Later in par. 7.3, it will be shown that this ratio is precisely the ratio of the variances of the estimates for these two cases.
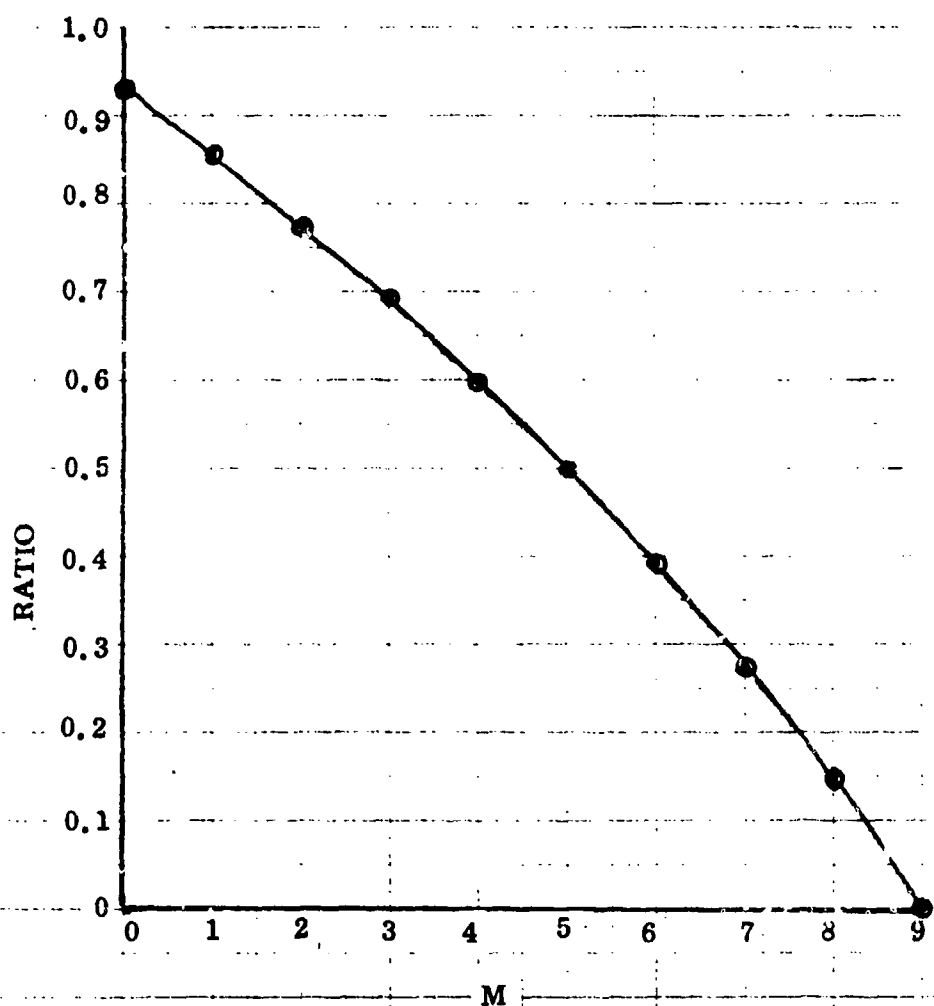
Figure 5-1. Ratio of Normalization Factors for Variance

MISSING DATA POINTS

The previous development implied evenly spaced data at every one of the N points. Because this procedure is to be used with real-world equipment with a probability of detection less the unity, it is clear that variance estimates will be required in regions having missing data points.

6.1 ORTHOGONAL POLYNOMIALS FOR MISSING DATA POINTS

Define a vector $\underline{H}$ with dimension N' that consists of N ones for N detections and $N' - N$ zeros for missed detections,

$$\underline{H} \triangleq \left[H_1 \; H_2 \; \ldots \; H_{N'} \right]^T,$$

$$(6-1)$$

with

$$N \triangleq \sum_{j=1}^{N'} H_j \; ; \qquad r \triangleq \sum_{j=1}^{r'} H_j \; ; \qquad s = \sum_{j=1}^{s'} H_j$$

$$(6-2)$$

where the relationships between r and r' and s and s' are the same for N and N'.

Moreover, define a quasi-identity matrix $\underline{I}'$ with $\underline{H}$ as its diagonal, i.e.

$$\underline{I}' \triangleq \begin{bmatrix} H_1 & & & \bigcirc \\ & H_2 & & \\ & & \ddots & \\ \bigcirc & & & H_{N'} \end{bmatrix} .$$

$$(6-3)$$

Then the variance estimate becomes,

$$\hat{\sigma}^2 = \frac{\tilde{\underline{Z}}'^T \tilde{\underline{Z}}'}{\text{Trace } \underline{\nu}'_{22}}$$

$$(6-4)$$

where

$$\underline{Z}' = \underline{I}' \underline{Z} \tag{6-5}$$

and

$$\text{Trace } \underline{\nu'_{22}} = \sum_{j=r'+1}^{s'} H_j - \sum_{k=1}^{M+1} \frac{\sum_{n=r'+1}^{s'} P_{nk}^2 H_n}{\sum_{n=1}^{N'} P_{nk}^2 H_n} \tag{6-6}$$

The polynomial set is orthogonal in domain N' with weighting matrix $\underline{H}$. The orthogonality relation is

$$\sum_{n=1}^{N'} P_{nk} P_{n\ell} H_n \begin{cases} 0 \; ; \; k \neq \ell \\ \\ \sum_{n=1}^{N'} P_{nk}^2 H_n \; ; \; k = \ell \; . \end{cases} \tag{6-7}$$

The recursion relation for these polynomials is

$$P_{j, k+1} = \left(j-1 - \beta_k \right) P_{jk} - \gamma_k P_{j, k-1} \; ; \quad 2 \leq k \leq M \tag{6-8}$$

with

$$\beta_k \triangleq \sum_{\ell=1}^{N'} (\ell-1) P_{\ell k}^2 H_\ell \Bigg/ \sum_{\ell=1}^{N'} P_{\ell k}^2 H_\ell , \tag{6-9}$$

$$\gamma_k \triangleq \sum_{\ell=1}^{N'} P_{\ell k}^2 H_\ell \Bigg/ \sum_{\ell=1}^{N'} P_{\ell, k-1}^2 H_\ell , \tag{6-10}$$

6-2

and

$$P_{j2} = j-1 - \left. \sum_{\ell=1}^{N'} (\ell-1) H_\ell \middle/ \sum_{\ell=1}^{N'} H_\ell \right. ,$$ (6-11)

$$P_{j1} = 1, \text{ for all } j .$$ (6-12)

Details of this set of orthogonal polynomials and its use can be found in Ref. (1).

6.2 COMPUTATIONAL EQUATIONS

These matrix forms of the equations for estimating variance from an incomplete data set, i.e., which include missing data points, have the following algebraic equivalents for computational purposes:

$$\hat{\sigma}_Z^2 = \frac{\sum_{i=r+1}^{s} H_j \left(Z_j - \hat{\hat{Z}}_j \right)^2}{\text{Trace } \underline{\nu}_{22}'}$$ (6-13)

while Trace $\underline{\nu}_{22}'$ is given by Equation (6-6) and

$$\hat{Z}_j = \sum_{k=1}^{M+1} \hat{b}_k H_j P_{jk}$$ (6-14)

with

$$\hat{b}_k = \frac{\sum_{\ell=1}^{N'} Z_\ell H_\ell P_{\ell k}}{\sum_{\ell=1}^{N'} P_{\ell k}^2} .$$ (6-15)

The expression for the adjacent point correlation coefficient in the face of missing data points is generalized to

$$\hat{\rho} = \frac{1}{\sigma^2} \left\{ \frac{\underline{\tilde{Z}'}^T \underline{U} \underline{\tilde{Z}'}}{N - M - 1} \right\} \tag{6-16}$$

or,

$$\hat{\rho} = \frac{\displaystyle\sum_{j=2}^{N'} \left(z_j - \hat{\bar{Z}}_j\right)\left(z_{j-1} - \hat{\bar{Z}}_{j-1}\right) H_j H_{j-1}}{\left\{ \displaystyle\sum_{j=2}^{N'-1} \left(z_j - \hat{\bar{Z}}_j\right)^2 H_j \sum_{j=2}^{N'} \left(z_j - \hat{\bar{Z}}_j\right)^2 H_j \right\}^{1/2}} \tag{6-17}$$

with Monte-Carlo simulation again demonstrating that

$$E\left(\hat{\rho}\right) = -\frac{M+1}{N} \; . \tag{6-18}$$

whenever $M \geq K$.

6-4

SECTION VII

STATISTICS OF THE VARIANCE ESTIMATE

It was shown earlier that the variance estimate is unbiased; that is the expectation value of the estimate is the true variance of the noise. Nevertheless the estimate itself is a random variable subject to uncertainty which arises primarily from three sources:

1. The assumption of a finite polynomial trend
2. Overfitting the trend
3. Insufficient sample size.

This section explains these sources of uncertainty and offers practical approaches to constraining them which have already been proven both by simulation and application to actual test flights.

7.1 POLYNOMIAL ASSUMPTION

Even a cartesian-linear flight path which doesn't overfly the radar will be trigonometric in the radar's polar coordinate system. Figures 7-1 and 7-2 show the range and azimuth histories of such a flight path with north offset of 10 nmi and asymptotic azimuth of 30°. In principle a polynomial fit to this data, particularly at close range would require an infinite number of terms. In practice, equivalent polynomial orders less than eight or nine are usually sufficient to fit mean flight paths down to a small fraction of the radar noise so long as two conditions are satisfied.

1. No range interval for estimating the mean target path extends beyond the point of closest approach.

2. These intervals must be adjusted downwards in length to accommodate the increasing curvature (in radar coordinates) encountered near the radar.

Both conditions stem from the fact that the equivalent polynomial order increases rapidly in the vicinity of the point of closest approach. An interval which straddles this point will require a much higher order of fit than one which places it at its boundary; thus the first condition. Nevertheless the reader is cautioned that this innermost interval may have to be broken up further, i.e., reduced in range extent, if the equivalent polynomial order of fit turns out to be too high for the computer being used. A 500-knot target with a radar having a revisit time of 12 seconds (5 rpm) will have about 6 data points in a 10-nmi range interval. Experience shows that a computer with 32-bit floating point capability can easily handle the 10-15th order polynomials sometimes required in the innermost 10-nmi range interval.
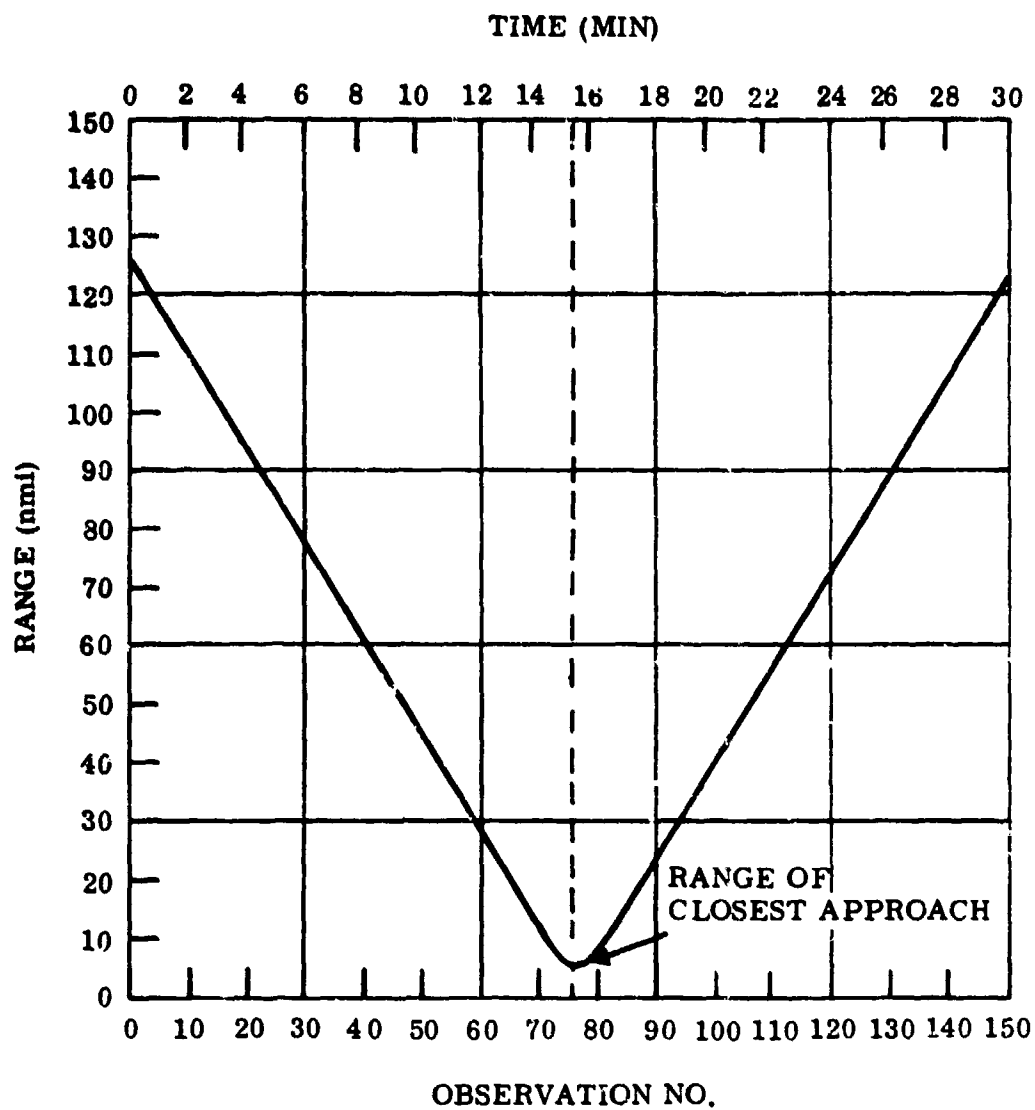
Figure 7-1. Range History for Cartesian Linear Flight Path
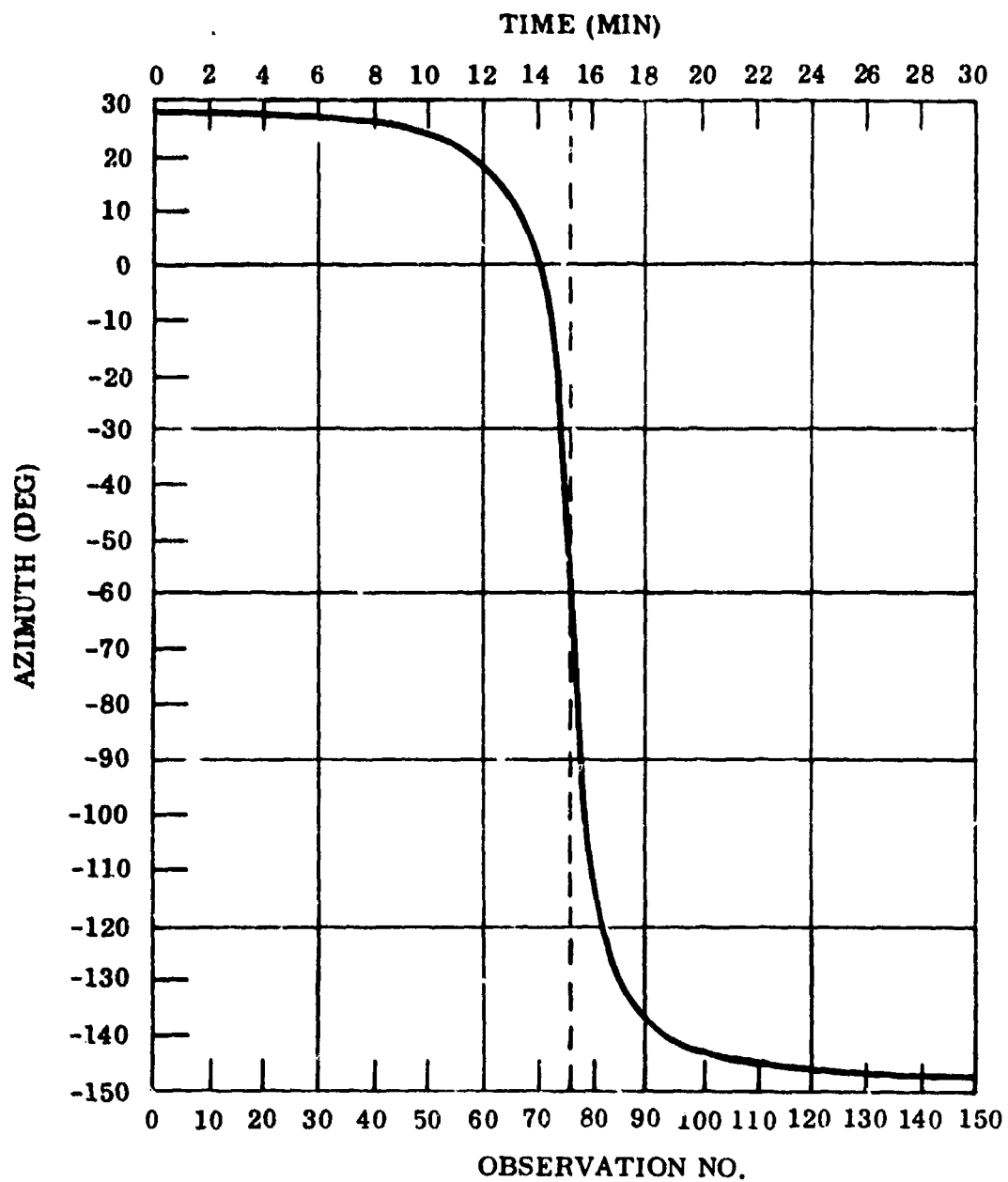with 10-nmi North Offset and Asymptotic
Azimuth of 30°

Figure 7-2. Azimuth History for Cartesian Linear Flight Path
with 10 nmi North Offset and Asymptotic
Azimuth of 30°

The second condition addresses the need to optimize the number of data points used in the fit, N, and the assumed polynomial order of fit, M, for a given set of data used for the variance estimate, L. The total flight path is usually divided into a number of intervals containing 6- to 10-data points a piece, i.e. L, starting with the point of closest approach to the radar. But there are two competing sources of error which require disparate optimal strategies for picking N and M. On the one hand, we'd like N as small as possible near the radar to minimize the true order of fit K, and thus avoid possible bias error from inadvertant underfitting in the region where the finite polynomial assumption begins to breakdown. On the other hand, it will be shown in par. 7.3 that increasing N for a given L and true order K will result in a dramatic decrease in the estimation uncertainty. After many simulations and the processing of much real data, the following strategy was derived which appears to provide a robust balance between these seemingly disparate requirements.

1. The order of fit M is increased from unity to the maximum permitted by the computation system with accuracy, and all those cases where the correlation coefficient is negative for M, M-1 and M-2 are accepted as legitimate variance estimates. The requirement that $\hat{\rho}$ be negative for M, M-1 and M-2 has been shown by experience to effectively eliminate the effects of sampling fluctuation on the instantaneous estimate $\hat{\rho}$ (M;N).

2. For ranges less than $4L\triangle R$ (where $\triangle R$ is the distance between data points) N=L and we pick the order of fit M to be the largest possible on the computer in use subject to the additional constraint on the correlation coefficient that $\hat{\rho}$ be negative for M+1 as well to provide additional assurance that the polynomial approximation is valid.

3. For ranges larger than $4L\triangle R$, N is systematically increased from L to 4L and M increased from the minimum established in step (1) to the maximum permitted by the accuracy of the computer (e.g. 10-15). The particular values of N and M used are those that correspond to the maximum Trace $\left(\nu'_{22} \right)$ [as calculated by Equation (6-6)] from the entire list of legitimate estimates.

4. The optimum strategy regarding the geometrical relationship between N and L is to use symmetry wherever possible, i.e. for L to be centered in N. This stems from the fact that while all possibilities will lead to unbiased (or minimally biased) estimates, the centered case results in the minimum estimation uncertainty. Near the ends of coverage or the point of closest approach L cannot be centered and some increased uncertainty must be tolerated.

Examples of the efficacy of these procedures are given in Appendices C and D.

7.2 DISTRIBUTION AND MOMENTS OF THE ESTIMAT.'

Basically the estimate of variance, as represented by Equation (6-13) can be viewed as a process whereby s-r Gaussian, zero-mean variates, i.e., $\tilde{Z}_j = Z_j - \bar{Z}_j$, are squared and summed, and then normalized by Trace ν_{22}'. Now it is commonly known that a random variable which is the sum of the squares of N independent zero-mean Gaussian variates is chi-square distributed with $\nu = N$ degrees of freedom. Moreover if the mean is estimated from averaging the data, then one degree of freedom is lost and $\nu = N-1$. It is a straightforward proof to show that when M+1 coefficients are required for the estimation of the mean then M+1 degrees of freedom are lost and $\nu = N-M-1$. For L=N then it is clear that

$$\hat{\sigma}^2 = \frac{\sigma^2 \chi_\nu^2}{\nu} . \tag{7-1}$$

where σ^2 is the true variance and ν the number of degrees of freedom of the random variable χ_ν^2. For L=N

$$\hat{\sigma}^2 = \frac{\sigma^2 \chi_\nu^2}{N-M-1} . \tag{7-2}$$

Since

$$E\left(\chi_\nu^2\right) = \nu \tag{7-3}$$

and

$$VAR\left(\chi_\nu^2\right) = 2\nu, \tag{7-4}$$

we see that

$$E\left(\hat{\sigma}^2\right) = \frac{\sigma^2}{N-M-1} E\left(\chi_\nu^2\right) = \sigma^2 \tag{7-5}$$

which shows again that the estimate is unbiased, and

$$VAR\left(\hat{\sigma}^2\right) = \left(\frac{\sigma^2}{N-M-1}\right)^2 VAR\left(\chi_\nu^2\right) = \frac{2\sigma^4}{N-M-1}, \tag{7-6}$$

which is a new result.

What happens when $N > L$ and $\nu = \text{Trace } \nu'_{22}$? With the proof in Appendix B, we state here that the normalized random variable $\text{Trace } \nu'_{22}\left(\widehat{\sigma^2} / \sigma^2\right)$ is still chi-square distributed with $\text{Trace } \nu'_{22}$ degrees of freedom. Thus,

$$\widehat{\sigma}^2 = \frac{\sigma^2 \, \chi^2_{\text{Trace } \nu'_{22}}}{\text{Trace } \nu'_{22}} . \tag{7-7}$$

From Equation (7-3),

$$E\left(\widehat{\sigma^2}\right) = \sigma^2$$

and

$$\text{VAR}\left(\widehat{\sigma^2}\right) = \frac{2\sigma^4}{\text{Trace } \nu'_{22}} . \tag{7-8}$$

Because $\text{Trace } \nu'_{22} > s-r-M-1$, as seen from Equation (5-8), it is easy to see that the uncertainty in the estimate is reduced by the procedure of using more points for the trend removal than for the variance estimate itself.

7.3 OVERFITTING THE TREND

It was already shown that overfitting does not introduce a bias. Nevertheless there is a penalty which appears as an increased uncertainty in the estimate. This may be seen clearly from Equation (7-6), which is the form of the variance of the estimate when $N=L$. The standard deviation of the estimate then varies almost inversely as the square root of order of fit, i.e.,

$$\text{SIG}\left(\widehat{\sigma^2}\right) = \text{SIG}\left(\widehat{\sigma_0^2}\right) = \sqrt{\frac{N-M_0-1}{N-M-1}} . \tag{7-9}$$

For $N=10$, Table 7-1 gives the increase in the standard deviation for the estimate with M_0 as the parameter.

TABLE 7-1

INCREASED UNCERTAINTY DUE TO OVERFITTING WHEN N=L=10

M \ M_0	0	1	2	3	4	5	6	7
1	1.06							
2	1.14	1.07						
3	1.22	1.15	1.08					
4	1.34	1.26	1.18	1.10				
5	1.50	1.41	1.32	1.22	1.12			
6	1.73	1.63	1.53	1.41	1.29	1.15		
7	2.12	2.00	1.87	1.73	1.58	1.41	1.22	
8	3.00	2.83	2.65	2.45	2.24	2.00	1.73	1.41

From this table, the uncertainty can almost triple when the true order is zero and increase by a factor of 2 when the true order is 5.

The general form of Equation (7-9), where $N \geq L$, is

$$\text{SIG}\left(\widehat{\sigma^2}\right) = \text{SIG}\left(\widehat{\sigma_0^2}\right) \sqrt{\frac{\text{Trace } \underline{\nu_{22}}\left(N, L, M_0\right)}{\text{Trace } \underline{\nu_{22}}\left(N, L, M\right)}} . \tag{7-10}$$

As a means of comparison, consider two examples. In both cases, we will keep L=10, analogous to the example from which Table 7-1 was constructed. Tables 7-2 and 7-3, on the other hand, present the results for N=20 and 40, respectively, where the L data points used for variance estimation are centrally located among the N data points used for trend removal.

7-7

TABLE 7-2

INCREASED UNCERTAINTY DUE TO OVERFITTING WHERE L=10 AND N=20

M \ M_o	0	1	2	3	4	5	6	7
1	1.007							
2	1.028	1.021						
3	1.051	1.044	1.022					
4	1.067	1.060	1.038	1.016				
5	1.092	1.085	1.062	1.039	1.023			
6	1.120	1.112	1.089	1.066	1.049	1.025		
7	1.143	1.136	1.112	1.088	1.071	1.047	1.021	
8	1.175	1.167	1.143	1.118	1.100	1.076	1.049	1.027

TABLE 7-3

INCREASED UNCERTAINTY DUE TO OVERFITTING WHERE L=10 AND N=40

M \ M_o	0	1	2	3	4	5	6	7
1	1.000							
2	1.015	1.015						
3	1.019	1.018	1.004					
4	1.031	1.030	1.015	1.012				
5	1.039	1.038	1.023	1.020	1.008			
6	1.048	1.047	1.032	1.028	1.017	1.009		
7	1.060	1.057	1.044	1.040	1.028	1.020	1.011	
8	1.067	1.067	1.051	1.047	1.035	1.027	1.018	1.007

It should be evident from these tables that the effect of increasing N for a given L are dramatic. For instance, when the true order is zero, the uncertainty barely increases by 18% for N=20 and 7% for N=40. Compare this to the 300% increase shown in Table 7-1. The length of these tables are kept to match Table 7-1 and not out of any theoretical restriction, recalling that

$$K \leq M \leq N-2 \qquad (7-11)$$

is the only restriction and we could have increased M to 18 for Table 7-2 and 38 for Table 7-4, if needed. The point here is that there is very little penalty for reasonable amounts of overfitting with $N > 2L$, leading to a robustness for the technique. In practice we have found that increasing N beyond 4L is unnecessary from the point of view of constraining the uncertainty in the estimate.

7.4 INSUFFICIENT SAMPLE SIZE

Because a typical air defense radar may only revisit a target once every 6 to 12 seconds, the total number of samples available for a variance estimate will be small on a single flight leg. As an example, a 500-knot target will yield only 6 unique data points in a 10-nmi range interval for a radar revisit time of 12 seconds. How big will the uncertainty in the estimate be? From Equation (7-8) we find that

$$\text{SIG} \left(\hat{\sigma}^2 \right) = \sqrt{\frac{2}{\text{Trace } \nu'_{22}}} \; \sigma^2 . \qquad (7-12)$$

For L=6, N=4L=24, $M_0 = 0$, and M=8 for example

$$\text{Trace } \nu_{22} = 4.54 .$$

Thus

$$\text{SIG} \left(\hat{\sigma}^2 \right) = 0.664 \, \sigma^2 \qquad (7-13)$$

which means that the uncertainty in the estimate of variance is larger than 65% of the true variance itself. From estimate-to-estimate then a considerable fluctuation will be encountered, perhaps far more that we would like.

One way to reduce this uncertainty is to extend the range interval, i.e. L, over which the estimate is made. This has several disadvantages. First, a large increase in L may force an averaging of true variance which may vary significantly over the range interval because at long range

$$\sigma^2 \propto R^4 .$$

Secondly, the pressure increases greatly for a higher order of fit than perhaps can be handled with precision on a typical computer.

An alternative approach which has proved quite effective in practice is to increase the number of flight legs for the same (or similar) conditions. Thus for p – flight legs where we average the variance estimates in like range intervals _after_ removing the trend on each leg.

$$\hat{\sigma}_p^2 = \frac{1}{p} \sum_{i\epsilon p} \hat{\sigma}_i^2 . \tag{7-14}$$

Note that the result is still unbiased, i.e.

$$E\left(\hat{\sigma}_p^2\right) = \sigma^2 . \tag{7-15}$$

Moreover,

$$VAR\left(\hat{\sigma}_p^2\right) = \frac{2\sigma^4}{p^2} \sum_{i\epsilon p} \frac{1}{Trace\left(\nu_{\underline{22}}\right)_i} . \tag{7-16}$$

For planning purposes, consider all N, L, and M identical from leg to leg for a given range interval.

Then,

$$VAR\left(\hat{\sigma}_p^2\right) = \frac{2\sigma^4}{p\ Trace\ \nu_{\underline{22}}} , \tag{7-17}$$

and

$$\text{SIG}\left(\hat{\sigma}_p^2\right) = \sqrt{\frac{2}{p \, \text{Trace} \, \nu_{22}}} \; \sigma^2 \; .$$

<div align="right">(7-18)</div>

Suppose, for the example just considered we wish to reduce $\text{SIG}\left(\hat{\sigma}_p^2\right)$ to only 30% of σ^2. Then from Equations (7-13) and (7-18), the number of legs required would be 5, not unreasonable. On the other hand, 44 legs would be required to reduce $\text{SIG}\left(\hat{\sigma}_p^2\right)$ to 30%, perhaps too many to justify economically.

This leads naturally into questions of test planning. What value of the ratio $\text{SIG}\left(\hat{\sigma}_p^2\right)$ is really appropriate? This is where the concept of statistical risk is useful; a subject treated in Section VIII.

7.5 UNCERTAINTY IN THE ESTIMATE OF STANDARD DEVIATION

From Equation (7-7) we see that the variance estimate is a random variable related to the chi-square variate with $\nu = \text{Trace} \; \nu_{22}^!$ degrees of freedom. Generalizing for p – flight legs then

$$\hat{\sigma}_p^2 = \frac{\sigma^2 \chi_{p\nu}^2}{p\nu}$$

<div align="right">(7-19)</div>

and

$$\hat{\sigma}_p \triangleq \sigma \sqrt{\frac{\chi_{p\nu}^2}{p\nu}} \; .$$

<div align="right">(7-20)</div>

Therefore,

$$\text{VAR}\left(\hat{\sigma}_p\right) \triangleq E\left\{\hat{\sigma}_p - E\left(\hat{\sigma}_p\right)\right\}^2 = E\left(\hat{\sigma}_p\right)^2 - E^2\left(\hat{\sigma}_p\right) \; .$$

But $E\left(\widehat{\sigma}_p\right)^2 = E\left(\widehat{\sigma}_p{}^2\right) = \sigma^2$, since the variance estimate is unbiased and

$$VAR\left(\widehat{\sigma}_p\right) = \sigma^2 - E^2\left(\widehat{\sigma}_p\right). \tag{7-21}$$

From Equation (7-20) and the chi-square pdf,

$$E\left(\widehat{\sigma}_p\right) = \frac{\displaystyle\int_0^\infty \sigma\left(\sqrt{\frac{t}{p\,\nu}}\right) t^{\frac{p\nu}{2}-1} e^{-\frac{t}{2}}\,dt}{2^{\frac{p\nu}{2}}\, \Gamma\left(\frac{p\nu}{2}\right)} = \sigma\sqrt{\frac{2}{p\nu}} \; \frac{\Gamma\left(\frac{p\nu+1}{2}\right)}{\Gamma\left(\frac{p\nu}{2}\right)} \tag{7-22}$$

Note that the expectation value of $\sqrt{\widehat{\sigma}_p{}^2}$, i.e. $\widehat{\sigma}_p$, is biased while $E^{1/2}\left(\widehat{\sigma}_p{}^2\right)$ is not. The thought arises that an alternate strategy could have been developed whereby we could have constructed an unbiased estimate of $\widehat{\sigma}_p$ in the first place from

$$\widehat{\sigma}_p \triangleq \frac{\Gamma\left(\frac{p\nu}{2}\right)}{\Gamma\left(\frac{p\nu+1}{2}\right)} \left\{ \frac{\underset{\sim}{Z}^T \underset{\sim}{Z}}{2/p\nu} \right\}^{1/2} . \tag{7-23}$$

The reason for not doing this is the desirability for combining estimates of the variance of the random component of error, as treated in this paper, with estimates of the variance of bias components, as estimated elsewhere (Ref. 2 for example). In this way, each variance estimate must itself be unbiased.

From Equations (7-21) and (7-22) then,

$$VAR\left(\widehat{\sigma}_p\right) = \sigma^2 \left\{ 1 - \frac{2}{p\nu} \left[\frac{\Gamma\left(\frac{p\nu}{2}+1\right)}{\Gamma\left(\frac{p\nu}{2}\right)} \right]^2 \right\} \tag{7-24}$$

7-12

and

$$\text{SIG}\left(\hat{\sigma}_p\right) = \left\{ 1 - \frac{2}{p\nu} \left[\frac{\Gamma\left(\frac{p\nu}{2} + 1\right)}{\Gamma\ \frac{p\nu}{2}} \right]^2 \right\}^{1/2} \qquad (7\text{-}25)$$

where

$$\nu \triangleq \text{Trace}\ \nu'_{\underline{\underline{22}}} \quad . \qquad (7\text{-}26)$$

Note that

$$\lim_{p\nu \to \infty} \frac{\Gamma\left(\frac{p\nu}{2} + 1\right)}{\Gamma\left(\frac{p\nu}{2}\right)} = \left(\frac{p\nu}{2}\right)^{1/2}$$

so that

$$\lim_{p\nu \to \infty}\ \text{SIG}\left(\hat{\sigma}_p\right) = 0$$

as expected.

SECTION VIII

STATISTICAL RISK AND CONFIDENCE BOUNDS

While the uncertainties in the estimate (variance or standard deviation) are useful in a comparative sense, they provide little direct information helpful in designing tests or evaluating test results. On the other hand, the concept of statistical risk is quite useful in designing tests to both constrain the producer's risk of falsely failing and to illuminate the spectrum of buyer's risks of falsely passing (as a function of his least acceptable performance); each deriving solely from insufficient sample sizes. Moreover, upper and lower confidence bounds can be derived to infer limits to truth implied by the test results. Analytical expressions for these concepts are derived here and numerical examples presented to illustrate their use.

8.1 DISTRIBUTION OF THE ESTIMATE

In the previous section, we stated that the distribution of the normalized variance estimate for one leg and range interval was chi-square with $\nu \triangleq$ Trace ν'_{22} degrees of freedom, i.e.,

$$f_{\chi^2_\nu}(t) = \frac{t^{\frac{\nu}{2}-1} \, e^{-\frac{t}{2}}}{2^{\frac{\nu}{2}} \, \Gamma\left(\frac{\nu}{2}\right)} \tag{8-1}$$

where

$$\chi^2_\nu = \nu \frac{\widehat{\sigma_c^2}}{\sigma^2} . \tag{8-2}$$

An estimate averaged over p legs, on the other hand, is not in general related to the chi-square variable because

$$\widehat{\sigma_p^2} = \frac{1}{p} \sum_{i \epsilon p} \widehat{\sigma_i^2} = \frac{\sigma^2}{p} \sum_{i \epsilon p} \frac{\chi^2_{\nu_i}}{\nu_i} . \tag{8-3}$$

Only when all $\nu_i = \nu$ is the estimate clearly still related to the chi-square variable, i.e.,

$$\widehat{\sigma_p^2} = \frac{\sigma^2}{p\nu} \sum_{i \epsilon p} \left(\chi^2_\nu\right)_i = \frac{\sigma^2}{p\nu} \chi^2_{p\nu} \tag{8-4}$$

with

$$f_{\chi^2_{p\nu}}(t) = \frac{t^{\frac{p\nu-1}{2}} e^{-\frac{t}{2}}}{2^{\frac{p\nu}{2}} \Gamma\left(\frac{p\nu}{2}\right)} .$$ (8-5)

Returning momentarily to the general formulation of Equation (8-3), we see that the distribution of $t = \chi^2_{\nu_1} / \nu_1$ is a special case of the gamma pdf, i.e.,

$$g_1(t) = \frac{1}{\beta_1^{a_1} \Gamma(a_1)} t^{a_1 - 1} e^{-t/\beta_1}$$ (8-6)

where

$$a_1 = \frac{\nu_1}{2}$$ (8-7)

and

$$\beta_1 = 1/a_1$$ (8-8)

which has a characteristic function,

$$\Phi_1(\omega) = \left[\frac{a_1}{a_1 - j\omega}\right]^{a_1} .$$ (8-9)

Because we are dealing with a summation over p such terms the characteristic function of σ_p^2 / σ^2 becomes,

$$\Phi_{\widehat{\sigma_p^2/\sigma^2}}(\omega) = \prod_{i \in p} \left[\frac{a_i}{a_i - j\omega}\right]^{a_i}$$ (8-10)

which has no known general inverse for arbitrary $\{a_i\}$ and p.

There are two reasons for needing the pdf in the general case,

1. To recompute pass/fail thresholds (par. 8.2) and buyer's limits (par. 8.3) after the test when the actual $\{\nu_i\}$ set will have been known in each range interval.

2. To compute relevant confidence bounds to true performance after the test as inferred by achieved performance and the actual $\{\nu_i\}$ set.

In lieu of an analytical distribution (general inverse to Equation (8-10), a histogram can be generated numerically after the specific set is known from a suitable chi-square random number generator structured according to the leg-averaged variance estimate, i.e., Equation (8-3). Another way is to numerically perform the inverse to the general characteristic function with a specific $\{\nu_i\}$ set; perhaps using a discrete Fourier transform, i.e.,

$$g_{\hat{\sigma}_p^2/\sigma^2}(t) = \int_{-\infty}^{\infty} \prod_{i \in p} \left(\frac{\nu_i/2}{\nu_i/2 - j\omega} \right)^{\nu_i/2} e^{-j\omega t} d\omega \tag{8-11}$$

so that,

$$\hat{g}_{\hat{\sigma}_p^2/\sigma^2}(k) = \Delta\omega \sum_{n=0}^{N-1} \prod_{i \in p} \left(\frac{\nu_i/2}{\nu_i/2 - j\omega_n} \right)^{\nu_i/2} e^{-j\omega_n k}, \tag{8-12}$$

$$k = 0, 1, 2, \ldots\ldots N-1,$$

where t is a sample of the $\hat{\sigma}_p^2/\sigma^2$ random variable and we evenly sample all of t-space at least 2N times. Note that when all $\{\nu_i\}$ are equal for each leg that

$$\beta = \frac{2}{\nu} \; ; \quad a = \frac{p\nu}{2} \tag{8-13}$$

so that the distribution becomes gamma with $p\nu = p$ Trace $\underline{\nu'_{22}}$ degrees of freedom. An example of this technique is shown in Appendix F.

8.2 PRODUCER'S RISK

The producer's risk is conceptually defined as the probability of his product failing a test when in truth it should have passed, i.e., falsely failing. Thus in terms of parameters of interest to us here,

$$R^p \triangleq P_r \left[\sigma_p^2 > \sigma_T^2 \;\middle|\; \sigma^2 \leq \sigma_T^2 \right] \tag{8-14}$$

where σ_T is the pass/fail threshold such that the producer passes the test if

$$\hat{\sigma}_p^2 \leq \sigma_T^2 . \tag{8-15}$$

It is a simple matter to express this risk mathematically as,

$$R^p = \int_{(\sigma_T/\sigma)^2}^{\infty} g_{\hat{\sigma}_p^2/\sigma^2} \left(t \;\middle|\; \sigma^2 \leq \sigma_T^2 \right) dt . \tag{8-16}$$

Figure 8-1 is a plot of this risk where all $\nu_i = \nu$ and the total number of degrees of freedom is

$$p\nu = p \, \text{Trace} \, \underline{\nu_{22}'} . \tag{8-17}$$

Noting that the abscissa is $\sigma_T/\sigma = \sqrt{\hat{\sigma}_p^2} / \sigma$, consider a producer's risk of 10%. If the number of degrees of freedom is only one, then the pass/fail threshold on $\sqrt{\hat{\sigma}_p^2}$, i.e., σ_T must be almost 65% more than the true value σ. This is the tolerance required to fairly accommodate the sampling fluctuation expected in the estimate while still leaving the producer with a 10% chance of falsely failing. If the buyer thinks this tolerance (or discrimination ratio) too large, he can insist on a larger sample size. In our case, this translates to more flight legs, i.e., increasing $p\nu$. Note that for $p\nu = 50$, the pass/fail threshold on $\sqrt{\hat{\sigma}_p^2}$ only has to be a little over 10% greater than the theoretical value σ.
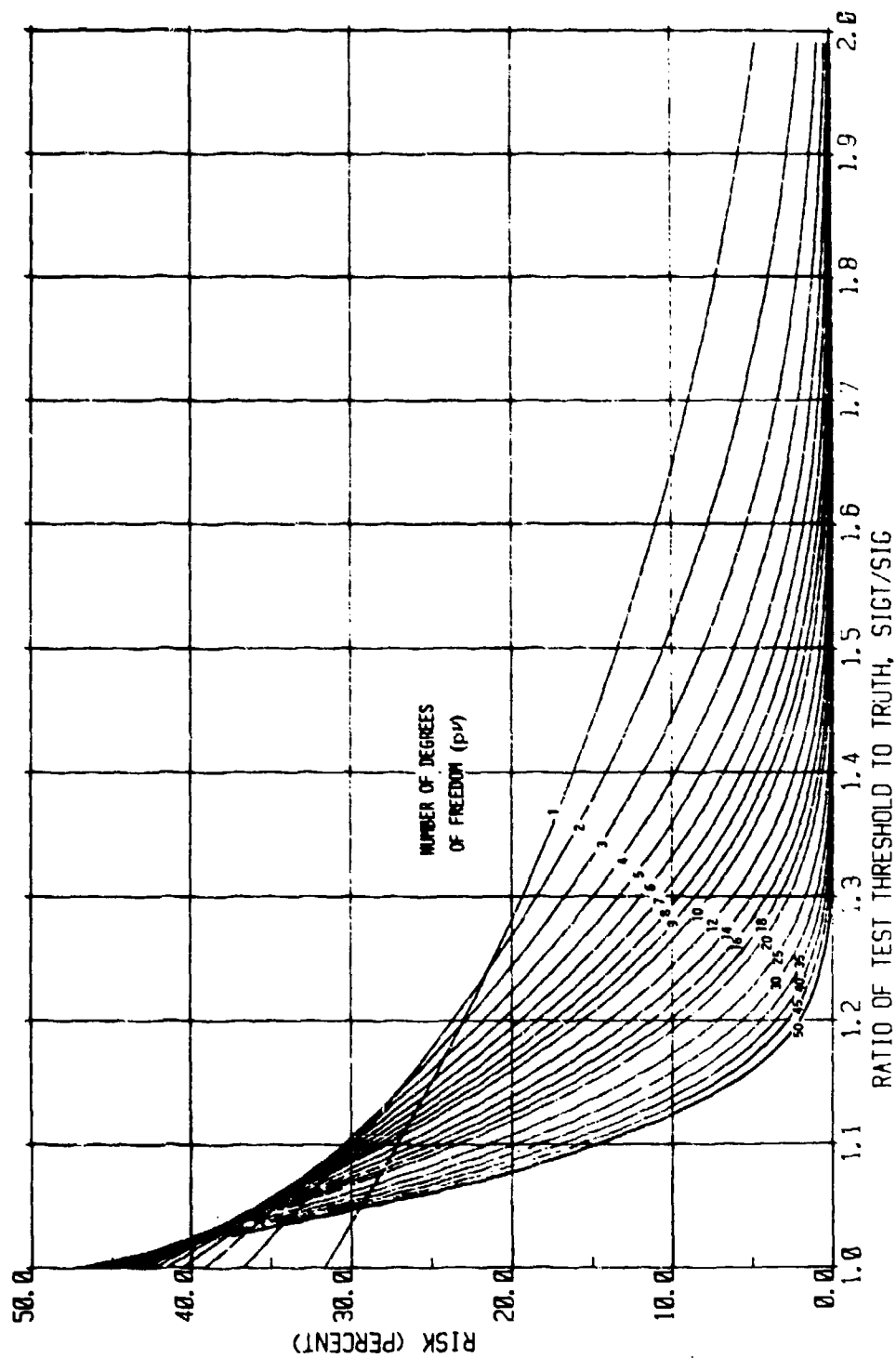
8-4

Figure 8-1. Producer's Risk of Falsely Failing an Acceptance Test

Because the pass/fail threshold is always related to the theoretical value, it is necessary to make an estimate of σ prior to the test. A reasonable candidate is the expected performance given that the product performs as promised. Thus the producer and the buyer must agree to this σ as part of the test package which includes the producer's risk, the number of flight legs, and other more mundane details of the test, e.g. altitude, speed, range interval, flight azimuth, etc. It is also important to relate these details to expected values for $\nu = \text{Trace } \nu'_{22}$. Figure 8-2 is helpful in this regard for it is a plot of ν for an eighth order polynomial fit against N as the independent variable and L as the parameter. Note that L is uniquely dependent on the speed of the aircraft and the revisit time of the radar under test and is assumed here to be centrally positioned with respect to $\{N\}$. The test planner can pick some representative value for $N \geq 2L$ and use the resulting ν for test planning purposes. For range intervals close to the radar, the value of ν used should probably be halved because of the increased pressure for higher order fits and the asymmetry of $\{L\}$ with respect to $\{N\}$.

8.3 BUYER'S RISK

The buyer's risk is conceptually defined as the probability of the product passing the test at the pass/fail threshold when in truth it should have failed at the limit of his acceptable performance, i.e., the buyer's limit. In terms of parameters of interest to us here,

$$R^B \triangleq P_r \left[\widehat{\sigma_p^2} \leq \sigma_T^2 \mid \sigma_B^2 > \sigma_T^2 \right] \tag{8-18}$$

Where σ_B is the buyer's limit which must be greater than both the pass/fail threshold σ_T and the theoretical or expected performance σ for the buyer's risk to be lower than about 50%. There is an asymmetry between the two risks shown here because it is the producer's product under test and the buyer's risk arises only because of his perception that $\sigma > \sigma_T$, which can never be known for sure. Once the parameters of the test are picked, i.e., R^P, p, E (Trace ν'_{22}), and σ, the pass/fail threshold is uniquely determined. But the buyer's limit is a parameter which can be traded off against the buyer's perceived risk. Figure 8-3 is helpful here in seeing this point. For $\sigma_T/\sigma_B = 0.5$ as an example, and $p\nu = 1$ the buyer's risk will be as high as 38%, but his penalty is 100%, i.e. $\sigma_B/\sigma_T - 1 = 1$. If p_ν is increased to 50, on the other hand, his perceived risk becomes vanishingly small, even though his penalty remains high. On the other hand, if he wishes to stand a risk of 10% with $p\nu = 50$ then the buyer may only have to accept a radar which is about 16% worse (i.e., $1/0.86 - 1$) than the test threshold, assuming that it passes the test. Compare this to the 100% penalty he must accept in the prior example where his risk is almost zero.
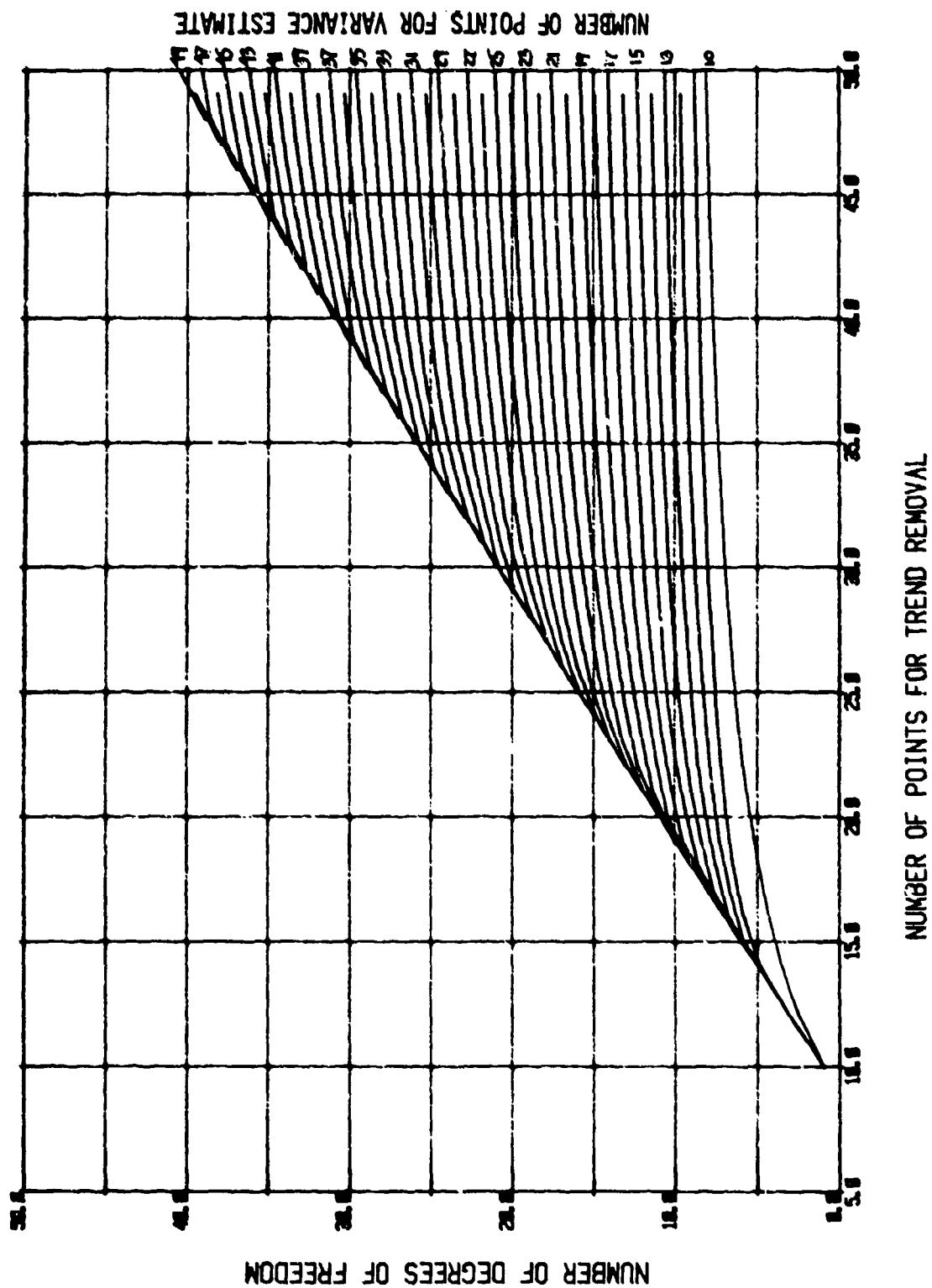
8-6

Figure 8-2. Number of Degrees of Freedom for a 8th Order Polynomial Trend
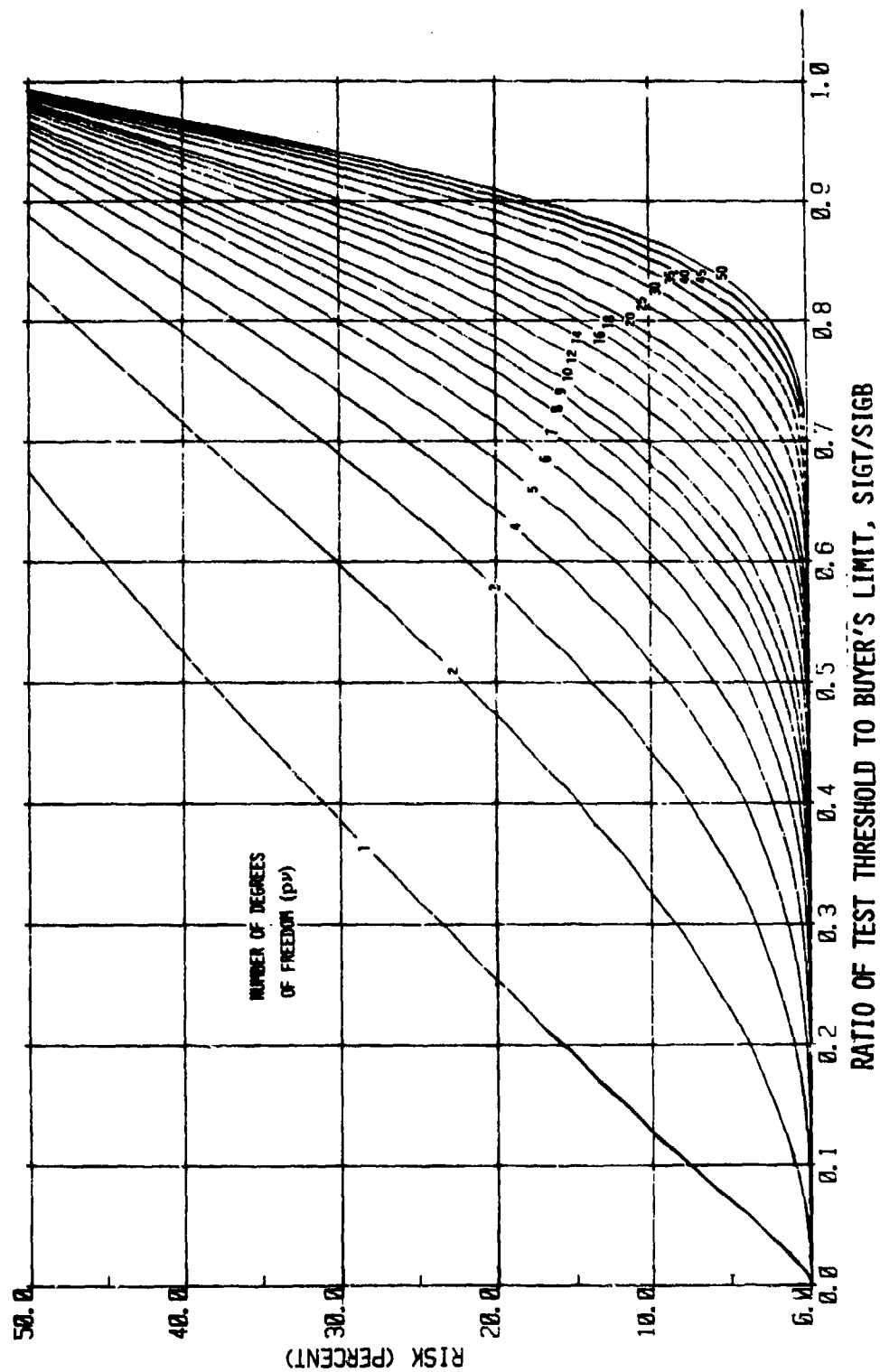
Figure 8-3. Buyer's Risk of Falsely Passing an Acceptance Test

8.4 CONFIDENCE BOUNDS

The concepts of producer's and buyer's risks are seen to be useful in providing tradeoffs to the design of effective, statistically meaningful tests, to the degree one can estimate expected performance, i.e., σ, prior to the test. Once the test is performed, it is natural to want to make inferences about the true performance implied by the test results.

A standard way of doing this is to provide upper and lower bounds to true performance, given the test result, associated on a one-to-one basis with a level of confidence. Figure 8-4 illustrates these bounds for the distribution of interest, i.e., Equation (8-13). With C the confidence level, a numerical solution is sought for σ_L and σ_H from

$$\int_{\hat{\sigma}_p^2 / \sigma_L^2}^{\infty} g_{\hat{\sigma}_p^2 / \sigma^2} \left(t \,\middle|\, \{\nu_i\} \right) dt \;=\; \frac{1-C}{2} \tag{8-19}$$

and

$$\int_{0}^{\hat{\sigma}_p^2 / \sigma_u^2} g_{\hat{\sigma}_p^2} \left(t \,\middle|\, \{\nu_i\} \right) dt \;=\; \frac{1-C}{2} \; . \tag{8-20}$$
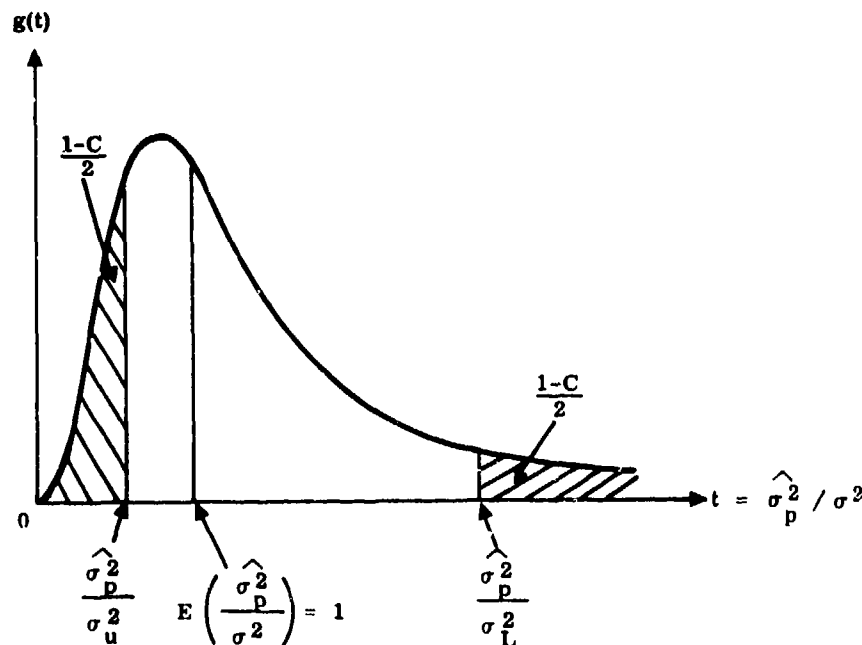

Figure 8-4. Distribution of the Variance Estimate Showing the Confidence Bounds of Interest

It is interesting to note that because the distribution is asymmetric, the bounds will be asymmetric as well. As an example, consider $p\nu = 10$ and $\sqrt{\hat{\sigma}_p^2} = 1$ kft. Then the square root of the 95% upper and lower confidence bounds for true variance are

$$\sigma_u = 2.16 \text{ kft}$$

and

$$\sigma_L = 0.63 \text{ kft}.$$

As another example, consider a tenfold increase in $p\nu$ to 100 with $\sqrt{\hat{\sigma}_p^2}$ still 1 kft. Then

$$\sigma_u = 1.26 \text{ kft},$$

and

$$\sigma_L = 0.856 \text{ kft}.$$

8.5 ADDITIONAL CONSIDERATIONS IN TEST DESIGN

Often an acceptance test on a radar may include five to ten separate performance measures, e.g. detection probability, height accuracy, range resolution, etc., several different altitudes, and 20 or more separate range intervals. The total number of independent tests may run up to the hundreds. If the producer's overall risk is to be kept to 10%, for example, and the criterion for passing is that he must pass all of say 100 tests, it should be obvious that his allocated risk per performance measure, per altitude, per range interval will be very small, i.e,

$$r^P = 1 - \left(1 - R^P\right)^{1/100} = 0.105\%.$$

The tolerance, i.e. σ_T/σ, will be much larger than for the single tests discussed in par. 8.2. Similarly, the buyer's risk per elemental subtest will be much higher than for the single test discussed in par. 8.3., i.e.,

$$r^B = \left(R^B\right)^{1/100} = 97.7\% ,$$

probably intolerable to most customers without considerable explanation. The reason for the dramatic telescoping of risks is the buyer's pass/fail criterion for passing the test; that is the producer must pass each and every elemental subtest to pass overall. A slight loosening of this criteria can pay dividends here. Suppose, for instance, that the producer can fail one or more, say m, subtests and still pass overall. Mathematically this is expressed as

$$R^P = \sum_{n=m+1}^{N_s} \frac{N_s !}{n! (N_s-n)!} \left(r^P\right)^n \left(1-r^P\right)^{N_s-n} \tag{8-21}$$

and

$$R^B = \sum_{n=N_s-m}^{N_s} \frac{N_s !}{n! (N_s-n)!} \left(r^B\right)^n \left(1-r^B\right)^{N_s-n} \tag{8-22}$$

where R^P and R^B are the overall test risks, r^P and r^B are the elemental subtest risks, N_s is the total number of subtests, and m is the number of permitted subtest failures.

These equations are solved numerically for r^P and r^B in Figures 8-5 and 8-6, respectively, for $R^P = R^B = 10\%$. As an example with $N_s = 100$ and $m = 10$ for example $r^P \approx 7\%$ and $r^B \approx 85\%$, somewhat better than for the case where no failures were permitted. Each test situation will demand its own tradeoffs and these ideas are only to focus attention on the procedures for effectively designing tests which are statistically fair to producer and buyer alike.
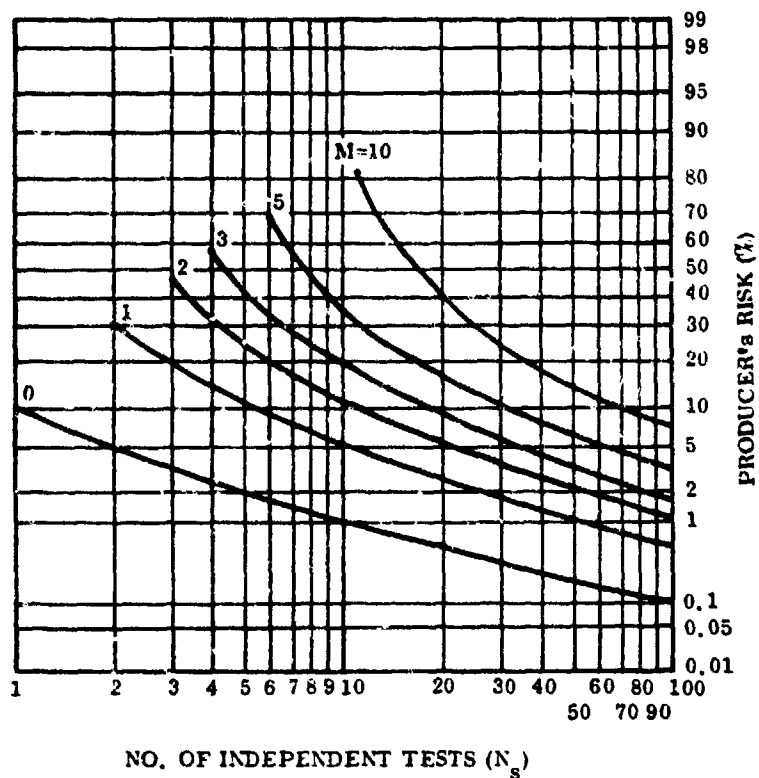
Figure 8-5. Producer's Risk per Test vs Total Number of Tests with Overall Risk of 10% and the Number of Permitted Failures as a Parameter
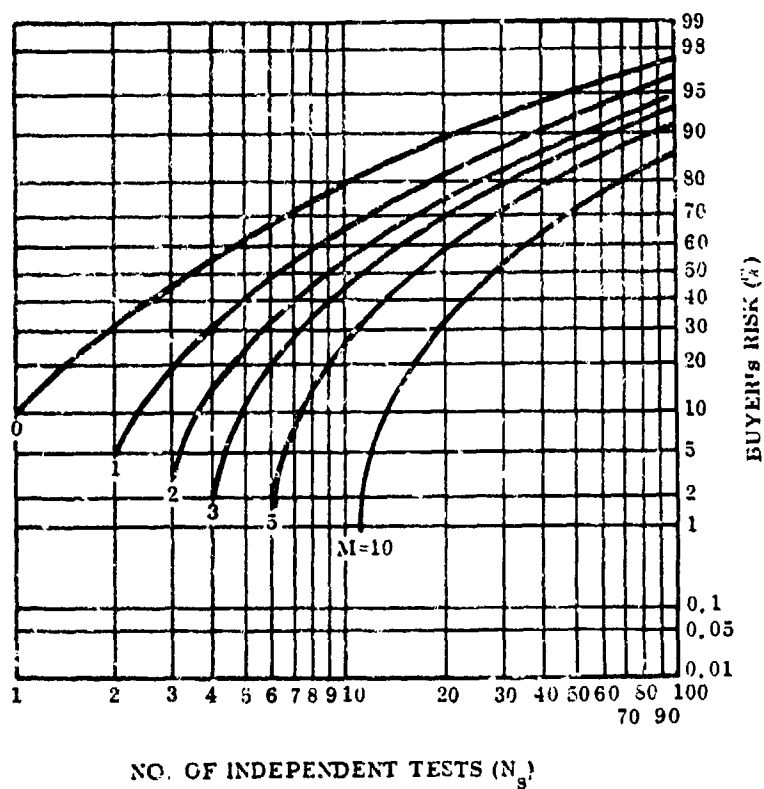
Figure 8-6. Buyer's Risk per Test vs Total No. of Tests with Overall Risk of 10% and the No. of Permitted Failures as a Parameter

SECTION IX

REFERENCES

1. S. D. Conte, C. deBoor, <u>Elementary Numerical Analysis, An Algorithmic Approach,</u> McGraw-Hill, 1980.

2. B. A. Deresh, <u>Radar Height Bias Estimation for a Ground Based Radar Using an Aircraft Altimeter as a Standard of Reference,</u> General Electric Technical Information is Series Report No. R82EMH3, June 1982.

APPENDIX A

DERIVATION OF THE TRACE ν_{22}

From Equation (5-5),

$$\underline{\nu} = (\underline{I} - \underline{M})^T (\underline{I} - \underline{M}) \tag{A-1}$$

where

$$\underline{M} = \underline{P} (\underline{P}^T \underline{P})^{-1} \underline{P}^T \tag{A-2}$$

and $\underline{P}$ is partitioned horizontally as,

$$\underset{(N \times M+1)}{\underline{P}} = \begin{bmatrix} \underline{P_1} \\ \text{-----} \\ \underline{P_2} \\ \text{-----} \\ \underline{P_3} \end{bmatrix} \begin{array}{l} (r \times M+1) \\ \\ (s-r \times M+1) \\ \\ (N-s \times M+1) \end{array} \tag{A-3}$$

resulting in a two-dimensional partition of $\underline{M}$ as

$$\underset{(N \times N)}{\underline{M}} = \begin{array}{ccc} (r) & (s-r) & (N-s) \\ \begin{bmatrix} \underline{M_{11}} & \underline{M_{12}} & \underline{M_{13}} \\ \underline{M_{21}} & \underline{M_{22}} & \underline{M_{23}} \\ \underline{M_{31}} & \underline{M_{32}} & \underline{M_{33}} \end{bmatrix} & \begin{array}{c} (r) \\ (s-r) \\ (N-s) \end{array} \end{array} \tag{A-4}$$

Defining

$$\underset{(M+1 \times M+1)}{\underline{\underline{B}}} \quad \triangleq \quad \underline{\underline{P}}^T \underline{\underline{P}} \tag{A-5}$$

one finds for orthogonal polynomials that the matrix is diagonal with elements

$$B_{kk} = \sum_{j=1}^{N} P_{jk}^2 \tag{A-6}$$

without any partitioning. The structure of $\underline{\underline{M}}$ is thus

$$\underline{\underline{M}} = \begin{bmatrix} \underline{P}_1 \underline{\underline{B}}^{-1} \underline{P}_1^T & \underline{P}_1 \underline{\underline{B}}^{-1} \underline{P}_2^T & \underline{P}_1 \underline{\underline{B}}^{-1} \underline{P}_3^T \\ \underline{P}_2 \underline{\underline{B}}^{-1} \underline{P}_1^T & \underline{P}_2 \underline{\underline{B}}^{-1} \underline{P}_2^T & \underline{P}_2 \underline{\underline{B}}^{-1} \underline{P}_3^T \\ \underline{P}_3 \underline{\underline{B}}^{-1} \underline{P}_1^T & \underline{P}_3 \underline{\underline{B}}^{-1} \underline{P}_2^T & \underline{P}_3 \underline{\underline{B}}^{-1} \underline{P}_3^T \end{bmatrix} \quad, \tag{A-7}$$

and

$$(\underline{\underline{I}} - \underline{\underline{M}}) = \begin{bmatrix} \underline{\underline{I}} - \underline{\underline{M}}_{11} & - \underline{\underline{M}}_{12} & - \underline{\underline{M}}_{13} \\ - \underline{\underline{M}}_{21} & \underline{\underline{I}} - \underline{\underline{M}}_{22} & - \underline{\underline{M}}_{23} \\ - \underline{\underline{M}}_{31} & - \underline{\underline{M}}_{32} & \underline{\underline{I}} - \underline{\underline{M}}_{33} \end{bmatrix} \quad . \tag{A-8}$$

A-2

Now

$$\underset{(N\times N)}{\nu_{22}} = \underset{(N\times s-r)}{(\underline{I} - \underline{M})_2^T} \; \underset{(s-r\times N)}{(\underline{I} - \underline{M})_2} \qquad\qquad \text{(A-9)}$$

and

$$\text{Trace } \nu_{22} = \text{Trace } (\underline{I} - \underline{M})_2^T \; (\underline{I} - \underline{M})_2$$

$$= \text{Trace } (\underline{I} - M)_2 \; (\underline{I} - \underline{M})_2^T \qquad\qquad \text{(A-10)}$$

$$= \text{Trace } \mu_{22} \, .$$

Thus the ij^{th} partitioning of μ is thus

$$\underline{\mu_{ij}} = \sum_{\ell=1}^{3} (\underline{I} - \underline{M})_{i\ell} \; (\underline{I} - \underline{M})_{\ell j}^T \qquad\qquad \text{(A-11)}$$

But only the diagonal elements of μ are needed for the Trace μ_{22}

and

$$\underline{\mu_{ii}} = (\underline{I} - \underline{M})_{i1} (\underline{I} - \underline{M})_{i1}^T + (\underline{I} - \underline{M})_{i2} (\underline{I} - \underline{M})_{2i}^T + (\underline{I} - \underline{M})_{i3} (\underline{I} - \underline{M})_{3i}^T \quad \text{(A-12)}$$

Specifically from Equation (A-8),

$$\underset{(s-r \times s-r)}{\mu_{22}} = \underset{(s-r \times r \times r \times s-r)}{M_{21} M_{12}} + \underset{(s-r \times s-r \times s-r \times s-r)}{(\underline{I} - M_{22})^2} + \underset{(s-r \times N-s \times N-s \times s-r)}{M_{23} M_{32}}$$

$$\text{(A-13)}$$

Expansion yields,

$$
\text{Trace } \underline{\nu}_{22} = \sum_{n=r+1}^{s} \sum_{i=1}^{r} \left[\sum_{k=1}^{M+1} \frac{P_{ik} P_{nk}}{B_{kk}} \right]^2
$$

$$
+ \sum_{n=r+1}^{s} \left\{ \left[1 - \sum_{k=1}^{M+1} \frac{P_{nk}^2}{B_{kk}} \right]^2 + \sum_{\substack{i=r+1 \\ i \neq n}}^{s} \left[\sum_{k=1}^{M+1} \frac{P_{ik} P_{nk}}{B_{kk}} \right]^2 \right\} \quad \text{(A-14)}
$$

$$
+ \sum_{n=r+1}^{s} \sum_{i=s+1}^{N} \left[\sum_{k=1}^{M+1} \frac{P_{ik} P_{nk}}{B_{kk}} \right]^2
$$

where the middle term reflects the different structure of the diagonal of $\underline{I} - \underline{M}$, noting that

$$
\mu_{nj} = \sum_{i=r+1}^{s} (\underline{I} - \underline{M})_{ni} \, (\underline{I} - \underline{M})_{ji}
$$

in general and

$$
\mu_{nj} = - M_{jn} \left(1 - M_{nn} \right) - M_{nj} \left(1 - M_{jj} \right) + \sum_{\substack{i=r+1 \\ i \neq n \\ i \neq j}}^{s} M_{ni} M_{ji}
$$

for $n \neq j$ and

$$
\mu_{nn} = \left(1 - M_{nn} \right)^2 + \sum_{\substack{i=r+1 \\ i \neq n}}^{s} M_{ni}^2 \quad \text{(A-15)}
$$

for $n = j$ in particular.

Combining the terms in Equation (A-14), adding and subtracting

$$\sum_{n=r+1}^{s} \left[\sum_{k=1}^{M+1} \frac{P_{nk}^2}{B_{kk}} \right]^2 ,$$

one gets

$$\text{Trace } \underline{\nu}_{22} = \sum_{n=r+1}^{s} \left\{ \sum_{i=1}^{N} \left[\sum_{k=1}^{M+1} \frac{P_{ik}\,P_{nk}}{B_{kk}} \right]^2 \right.$$

$$\left. + \left[1 - \sum_{k=1}^{M+1} \frac{P_{nk}^2}{B_{kk}} \right]^2 - \left[\sum_{k=1}^{M+1} \frac{P_{nk}^2}{B_{kk}} \right]^2 \right\} . \qquad (A-16)$$

Defining

$$\psi_{in} \triangleq \left[\sum_{k=1}^{M+1} \frac{P_{ik}\,P_{nk}}{B_{kk}} \right]^2 = \sum_{k} \left(\frac{P_{ik}\,P_{nk}}{B_{kk}} \right)^2 + 2\,\frac{P_{i1}\,P_{n1}}{B_{11}} \left(\frac{P_{i2}\,P_{n2}}{B_{22}} + \cdots + \frac{P_{i,M+1}\,P_{n,\,M+1}}{B_{M+1,\,M+1}} \right)$$

$$+ \text{------------------} + 2\,\frac{P_{iM}\,P_{nM}}{B_{MM}}\,\frac{P_{i,\,M+1}\,P_{n,\,M+1}}{B_{M+1,\,M+1}} ,$$

then

$$\sum_{i=1}^{N} \psi_{in} = \sum_{i=1}^{N} \sum_{k=1}^{M+1} \left(\frac{P_{ik}\,P_{nk}}{B_{kk}} \right)^2 = \sum_{k=1}^{M+1} \frac{P_{nk}}{B_{kk}}$$

from successive application of the orthogonality relations [Equation (4-5)] .

Introducing this result into Equation (A-16), expanding and cancelling terms,

$$\text{Trace } \nu_{\underline{22}} = \sum_{n=r+1}^{s} \left\{ 1 - \sum_{k=1}^{M+1} \frac{P_{nk}^2}{B_{kk}} \right\}$$

and finally with the definition of B_{kk},

$$\text{Trace } \nu_{\underline{22}} = s-r - \sum_{k=1}^{M+1} \frac{\displaystyle\sum_{n=r+1}^{s} P_{nk}^2}{\displaystyle\sum_{n=1}^{N} P_{nk}^2} \, . \qquad\qquad (A-17)$$

APPENDIX B

DISTRIBUTION FOR THE PARTITIONED DATA SET

From Equations (6-4) and (5-6A), we have that

$$\hat{\sigma}^2 = \frac{\tilde{\underline{z}}'^T \tilde{\underline{z}}'}{\text{Trace } \nu'_{22}} = \frac{\underline{v}'^T \nu'_{22} \underline{v}'}{\text{Trace } \nu'_{22}} \tag{B-1}$$

so that

$$E\left(\hat{\sigma}^2\right) = \sigma^2. \tag{B-2}$$

In general, the estimate of variance involves the summation of L=N squares of partially correlated zero-mean Gaussian variables. Zero-correlation (totally independent variables) requires that each variable be zero-mean a priori. In this case, the estimate is chi-square distributed with L degrees of freedom. Unity correlation (completely dependent variables) requires that each variable be essentially the same. In the case, the estimate is still chi-square, but with 1 degree of freedom. Moreover we have seen that estimation of an Mth order polynomial trend model uses up M+1 degrees of freedom, partially correlating the data in the process. In this case, the estimate is chi-square distributed with L-(M+1) degrees of freedom. In summary, the summation of L squared zero-mean, partially correlated, Gaussian variables always leads to a chi-square distribution with $\nu = L - x$ degrees of freedom. For the partitioned case, L = s-r and

$$x = \sum_{k=1}^{M+1} \frac{\sum_{j=r+1}^{s} P_{jk}}{\sum_{j=1}^{N} P_{jk}}. \tag{B-3}$$

Note that x = 0 for $\rho = 0$ and x = L-1 for $\rho = -1$, i.e., M = N-1.

With this line of reasoning, we can use Equation (B-1) to redefine the variance estimate as

$$\hat{\sigma}^2 = \frac{\sigma^2 \chi^2_\nu}{\text{Trace } \nu'_{\underline{22}}} \, .$$

(B-4)

Thus,

$$E(\hat{\sigma}^2) = \frac{\sigma^2}{\text{Trace } \nu'_{\underline{22}}} \, E(\chi^2_\nu) = \frac{\sigma^2 \nu}{\text{Trace } \nu'_{\underline{22}}} \, .$$

(B-5)

From Equations (B-2) and (B-5) then

$$\nu = \text{Trace } \nu'_{\underline{22}} \, ,$$

(B-6)

the number of degrees of freedom for the general case.

APPENDIX C

MONTE-CARLO SIMULATIONS TO VALIDATE THE TECHNIQUE

Many simulations were performed to help validate the technique in increasingly realistic steps. The common elements of each simulation were as follows:

1. Gaussian noise was added to simple models for the mean flight path (trend).

   - independent samples

   - representative models for radar measurement noise including range dependent and range independent components.

2. The target was assumed to have a constant speed and mean cross section, typical of small military aircraft.

3. The radar rotated at 5 rpm and was assumed to have typical signal processing features and radar coverage.

Two simulations will be reported which both illustrate the value and validity of specific features of the technique developed here and demonstrate its robustness as well.

C.1 TRENDS OF KNOWN AND CONSTANT POLYNOMIAL ORDERS

The first simulation of interest is one in which the mean flight path was linear in range and constant in azimuth, i.e. truly radial, so as to provide a closely controlled test. Each data interval included L=10 points for the variance estimate and N=30 points for the trend removal process. A detection probability of 90% was assumed at all ranges and 500 Monte-Carlos were performed. Each Monte-Carlo was independent, whereby samples were drawn first from Gaussian random number generators scaled for range and azimuth position errors, and then from a uniform random number generator (simulating a 90/10 coin flip) to determine radar detectability. After a 30-point data set was assembled, the estimation process was initiated and the autocorrelation and variance estimates were stored. This process was repeated 500 times (all independent) and the estimates averaged to approximate an expectation value. Typical results are shown in Table C-1.

TABLE C-1

RESULTS OF SIMULATION WITH A KNOWN AND CONSTANT TREND MODEL

The upper set of tables show the actual range and azimuth of the aircraft, and the noise models for root-track position variance used to scale the Gaussian random number generators at each range point. Data points 11 through 20 have asterisks indicating those used to estimate variance. The lower set of tables show the results versus assumed order of fit. These tables are grouped first for range measurement and second for azimuth measurement. Within each grouping are two tables, the first summarizing performance in estimating the adjacent point autocorrelation function and the second summarizing performance in estimating the root-variance of radar measurement error. Both truth (which we know with certainty in this case) and results (labeled "expected") are given for comparison. The following summarizes the results:

1. In all cases where the correlation coefficient is negative, the root-variance estimates are excellent, exhibiting the level of deviation from truth expected from the sample size of 500.

2. The correlation coefficient goes negative for a first order fit in range and a zero order fit for azimuth, as predicted.

3. All estimates with overfitting are excellent with very little growth seen in the standard deviations of estimation error, as indicated by the "+/-" symbols.

4. The Monte-Carlo calculated values for uncertainty in the variance estimate are very close to theoretical expectation. For example consider M=8. From Figure 8-2 with N=30 and L=10, $\nu \approx 7$. From Equation (7-8),

$$\text{VAR} \, (\widehat{\sigma^2}) = \frac{2\sigma^4}{\nu} \, . \tag{C-1}$$

From Table C-1 and M=8, σ_R = 114.3 ft and σ_A = 1.682 mrad. Then from Equation (C-1),

$$\text{VAR}^{1/4} \, (\widehat{\sigma^2}) \left\{ \begin{array}{l} 83.6 \text{ ft} \\ 1.23 \text{ mrad} \end{array} \right.$$

which compare quite favorably to the Monte-Carlo results reported, i.e., 81.1 ft and 1.213 respectively.

C.2 COMPLEX TRIGOMETRIC TREND MODELS

An example is given here of a Monte-Carlo simulation that was actually used as an acceptance test for the data reduction technique by a GE customer. An aircraft was simulated to be flying at 40 kft at a speed of 487 knots. It flew 10 east-west legs out to 200 nmi with a north offset of 0.5 nmi. The actual aircraft flight path oscillated about the radial in both plan-position and height according to the following equations:

$$N = 0.5 \text{ nmi} + 0.0234 \text{ SIN } (42.7 \text{ E} + \phi_1) \tag{C-2}$$

$$H = 40,000 \text{ ft} + 300 \text{ SIN } (43.2 \text{ E} + \phi_2) \tag{C-3}$$

where

E = distance east of the radar (nmi)
N = distance north of the radar (nmi)
ϕ = arbitrary phase angles (deg), and
H = altitude (ft) .

At the start of each leg, the phase was reinitialized independently for distance and altitude. The maximum aircraft amplitude deviation from radial was 142 ft with a period of 62.3 s (8.43 nmi). The maximum amplitude deviation in height was 300 ft with a period of 61.57 s (8.33 nmi).

On top of this mean aircraft motion was measurement noise drawn independently point-to-point from a Gaussian random number generator scaled to a typical model for noise vs range.

Pass/fail thresholds were calculated based on a 1% risk of falsely failing due to statistical uncertainty. Sixty tests were made in all (20 range intervals each for range, height, and azimuth). The results are given in Tables C-2, C-3, and C-4 for range, height, and azimuth, respectively. The first two columns give the range intervals. The second column shows the theoretical standard deviation of measurement error from which the noise was added to the data. The fourth column gives the estimates made by the technique described here and the last column presents the pass/fail thresholds.

TABLE C-2

SIMULATION RESULTS FOR
RANGE ACCURACY

R1 (NMI)	R2	THEORY (FEET)	PASS/FAIL (FEET)	ESTIMATION (FEET)
4.	14.	60.7	88.4	54.9
10.	20.	60.7	88.4	60.7
20.	30.	60.8	88.6	49.8
30.	40.	61.2	89.1	65.1
40.	50.	62.1	90.3	56.3
50.	60.	63.6	92.6	58.9
60.	70.	66.1	96.2	62.8
70.	80.	69.8	101.7	67.9
80.	90.	75.0	109.2	72.4
90.	100.	82.4	120.0	86.1
100.	110.	91.7	133.5	92.8
110.	120.	102.0	148.5	104.8
120.	130.	113.9	165.8	128.6
130.	140.	127.4	185.4	141.3
140.	150.	142.3	207.1	141.2
150.	160.	158.7	231.0	173.5
160.	170.	178.1	259.2	171.0
170.	180.	199.0	289.6	181.8
180.	190.	219.6	319.7	223.2
189.	199.	239.5	348.5	247.6

TABLE C-3

SIMULATION RESULTS FOR
HEIGHT ACCURACY

R1 (NMI)	R2	THEORY (FEET)	PASS/FAIL (FEET)	ESTIMATION (FEET)
4.	14.	124.5	181.3	178
10.	20.	163.7	238.3	209
20.	30.	248.4	361.5	267
30.	40.	345.6	503.0	384
40.	50.	444.1	646.3	501
50.	60.	536.3	780.5	598
60.	70.	629.3	915.9	594
70.	80.	723.2	1052.5	680
80.	90.	818.1	1190.6	844
90.	100.	922.6	1342.7	926
100.	110.	1028.9	1497.5	993
110.	120.	1129.7	1644.2	1204
120.	130.	1233.7	1795.5	1431
130.	140.	1341.6	1952.5	1348
140.	150.	1454.2	2116.5	1397
150.	160.	1572.7	2288.8	1673
160.	170.	1709.0	2487.3	1729
170.	180.	1854.3	2698.8	1754
180.	190.	1998.5	2908.6	1910
189.	199.	2138.0	3111.6	1873

TABLE C-4

SIMULATION RESULTS FOR
AZIMUTH ACCURACY

R1 (NMI)	R2	THEORY (MRAD)	PASS/FAIL (MRAD)	ESTIMATION (MRAD)
4.	14.	1.998	2.907	2.59
10.	20.	1.998	2.907	2.26
20.	30.	1.998	2.908	2.05
30.	40.	1.998	2.908	2.12
40.	50.	2.000	2.910	1.89
50.	60.	2.002	2.914	1.91
60.	70.	2.006	2.920	1.93
70.	80.	2.012	2.929	1.79
80.	90.	2.022	2.942	1.90
90.	100.	2.036	2.963	1.97
100.	110.	2.055	2.992	2.06
110.	120.	2.079	3.026	2.14
120.	130.	2.110	3.071	2.12
130.	140.	2.148	3.126	2.33
140.	150.	2.194	3.193	2.21
150.	160.	2.249	3.273	2.09
160.	170.	2.320	3.376	2.21
170.	180.	2.402	3.496	2.32
180.	190.	2.490	3.624	2.54
189.	199.	2.579	3.753	2.85

The a priori expectation of falsely failing one of the 60 tests is the risk times the number of tests, i.e., 1% x 60 = 60%. It is interesting that no failures occured. This is indeed remarkable particularly for height accuracy close to the radar where the amplitude of the real aircraft motion was almost three times larger than the rms noise level.

APPENDIX D

SAMPLE RESULTS FOR A REAL FLIGHT TEST

In Appendix C we saw how well the technique worked for simulated flight trends with known and constant polynomial orders on the one hand and complex trigonometric paths of variable and unknown order on the other. In the first case, 500 Monte-Carlos were performed so that the estimation error was small. In the second example, 10 flight legs were averaged, equivalent to 10 Monte-Carlos, and the larger fluctuations were accommodated by pass/fail thresholds calculated from the risk concepts of Section VIII. Here we show results for a single range interval and a single leg (1-Monte-Carlo) from an actual flight test using a Lear jet on a near-radial flight path.

Figure D-1 shows one leg that we will examine in detail. Tables D-1, D-2, and D-3 summarize the results for the interval between 30 and 40 nmi for range, azimuth, and height errors respectively, versus assumed order of fit. Because we have in effect only one Monte-Carlo these are instantaneous estimates, not expectation values. It is not surprising then to see reasonable estimates corresponding to positive values of correlation coefficient. Nevertheless the following conclusions may be drawn from this example:

1. For all three coordinates, an asymptotic estimate is reached with remarkably low fluctuation.

2. The coordinates start off with truly poor estimates when the instantaneous correlation coefficient is above 0.8.

3. Even though the pilot was attempting to fly a constant height, radial flight path (i.e., $K_R = 1$, $K_A = 0$, $K_4 = 0$) the estimates for these implied orders of fit are truly poor.

4. Estimates of the theoretical values are:

$$\sigma_R = 114 \text{ ft}$$
$$\sigma_A = 0.79 \text{ mrad}$$
$$\sigma_H = 229 \text{ ft}$$
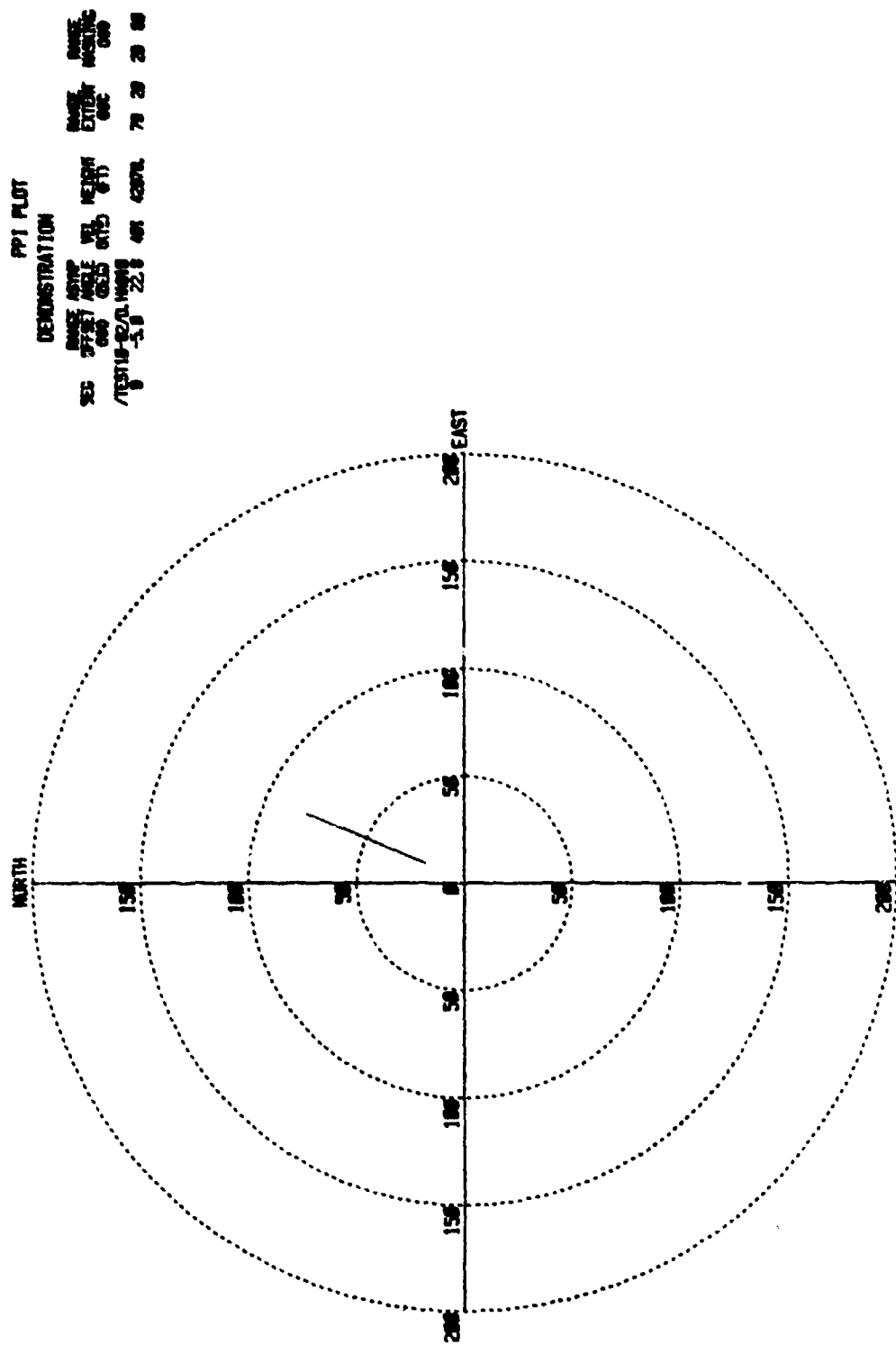
Figure D-1. PPI Plot (One Leg)

Note that by applying the rule for picking the best estimate at ranges less than 40 nmi (see par. 7.1), estimates are chosen with the fewest points, N, and the highest order of fit such that negative autocorrelations are achieved for M-1, M and M+1. From Tables D-1, D-2, and D-3 then the selected estimates are:

$$\hat{\sigma}_R = 150 \text{ ft}$$

$$\hat{\sigma}_A = 0.86 \text{ mrad}$$

$$\hat{\sigma}_H = 205 \text{ ft}$$

which are not bad for instantaneous estimates.

TABLE D-1

RANGE ERROR ESTIMATION FOR 30-40 nmi RANGE INTERVAL
N=L=8

M	CORR	SIGMA (FEET)	TRACE
0	0.883	19583.7	7.00
1	-0.426	117.6	6.00
2	-0.502	122.2	5.00
3	-0.459	131.7	4.00
4	-0.548	149.5*	3.00
5	-0.645	159.9	2.00

*This is the selected estimate.

TABLE D-2

AZIMUTH ERROR ESTIMATION FOR 30-40 nmi RANGE INTERVAL
N=L=8

M	CORR	SIGMA (MRAD)	TRACE
0	0.834	3.900	7.00
1	-0.663	0.693	6.00
2	-0.729	0.755	5.00
3	-0.733	0.836	4.00
4	-0.677	0.857*	3.00
5	-0.726	1.030	2.00

*This is the selected estimate.

TABLE D-3

HEIGHT ERROR ESTIMATION FOR 30-40 nmi RANGE INTERVAL

N=L=8

M	CORR	SIGMA (FEET)	TRACE
0	0.162	231.5	7.00
1	-0.114	194.2	6.00
2	-0.058	206.3	5.00
3	-0.392	204.0	4.00
4	-0.393	204.8*	3.00
5	-0.629	65.6	2.00

*This is the selected estimate.

Figure D-2 shows all of the legs combined for this flight test. Unfortunately for the (30-40 nmi) range interval there were only 2 legs. The estimates are:

$$\hat{\sigma}_R = 115 \text{ ft}$$

$$\hat{\sigma}_A = 0.862 \text{ mrad}$$

$$\hat{\sigma}_H = 236 \text{ ft}$$

in some cases closer to our theoretical expectations. To demonstrate that these estimates are truly consistent with theory within the limits of sampling-induced uncertainty, consider that the sum of the 2 traces from Tables D-1, D-2, and D-3 are 14.3, 14.8, and 15.7 respectively. The square-root of the upper and lower 90% confidence bounds to the above estimates are shown below as bracketing theory in all these cases.

RANGE

$$88.4 \leq 114 \text{ ft} \leq 168$$

AZIMUTH

$$0.663 \leq 0.79 \text{ mrad} \leq 1.26$$
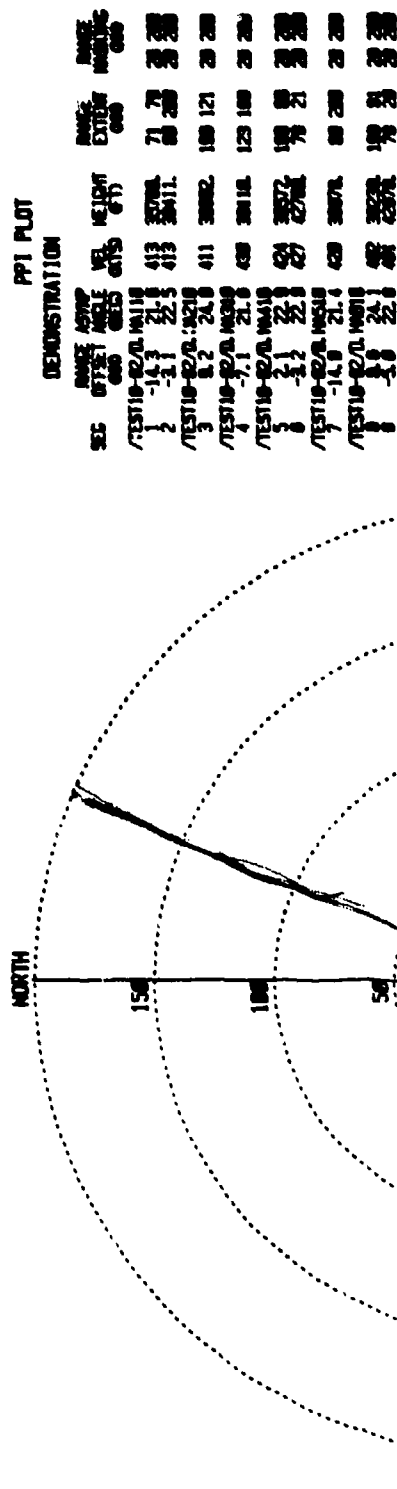
HEIGHT

$$183 \leq 229 \text{ ft} \leq 339 .$$

Figure D-2. PPI Plot (All Legs Combined)

As an example of the method used beyond 40 nm, based on the leg plotted in Figure D-1, Tables D-4, D-5, and D-6 summarize the results for the interval between 50 and 60 nmi for range, azimuth, and height errors respectively versus the best estimate for each number of points, N, from L to 4L.

The estimates of the theoretical values for this case are:

$$\sigma_R = 114 \text{ ft}$$

$$\sigma_A = 0.4 \text{ mrad}$$

$$\sigma_H = 310 \text{ ft}$$

This time the rule for picking the best estimate at ranges greater than 40 nmi is applied (see par. 7.1). For each number of points, candidates are chosen with the minimum order of fit, M, such that negative autocorrelations are achieved for M-2, M-1 and M. The candidate with the maximum trace is then chosen as the best estimate. For Tables D-4, D-5, and D-6, the best estimates are:

$$\hat{\sigma}_R = 121 \text{ ft}$$

$$\hat{\sigma}_A = 0.45 \text{ mrad}$$

$$\hat{\sigma}_H = 241 \text{ ft}$$

Again, from Figure D-2, only two legs (p=2) were available for this range interval (50-60 nmi) with the 2-leg average given as:

$$\hat{\bar{c}}_R = 93.7 \text{ ft}$$

$$\hat{\bar{\sigma}}_A = 0.411 \text{ mrad}$$

$$\hat{\bar{\sigma}}_H = 237.6 \text{ ft}$$

TABLE D-4

RANGE ERROR ESTIMATION FOR 50-60 nmi RANGE INTERVAL

	CORR (M-3)	CORR (M-2)	CORR (M-1)	CORR (M)	M	SIGMA (FEET)	TRACE
8	0.382	-0.250	-0.250	-0.513	3	140.6	4.00
9	0.909	-0.241	-0.246	-0.263	3	136.6	4.86
10	0.927	-0.235	-0.235	-0.192	3	130.3	5.65
11	0.941	-0.331	-0.292	-0.304	3	125.6	5.87
12	0.951	-0.205	-0.244	-0.242	3	126.5	6.07
13	0.959	-0.095	-0.295	-0.281	3	124.1	6.24
14	0.103	-0.255	-0.258	-0.334	4	124.3	6.01
15	0.164	-0.283	-0.278	-0.376	4	122.5	6.17
16	0.324	-0.267	-0.267	-0.355	4	122.5	6.33
17	0.430	-0.323	-0.319	-0.370	4	122.0	6.45
18	0.540	-0.316	-0.321	-0.350	4	122.1	6.55
19	0.554	-0.157	-0.230	-0.214	4	123.3	6.62
20	0.637	-0.150	-0.222	-0.212	4	122.8	6.70
21	0.617	-0.144	-0.283	-0.290	4	120.9	6.76
22	0.600	-0.162	-0.145	-0.228	4	128.5	6.82
23	0.635	-0.158	-0.173	-0.216	4	128.0	6.87
24	0.580	-0.263	-0.253	-0.369	4	121.1	6.92
25	0.599	-0.277	-0.283	-0.340	4	121.3	6.96
26	0.656	-0.303	-0.303	-0.364	4	121.9	7.00
27	0.693	-0.312	-0.325	-0.373	4	121.4	7.03
28	0.722	-0.293	-0.293	-0.374	4	121.0	7.06
	0.739	-0.309	-0.308	-0.371	4	122.0	7.09
30	0.764	-0.293	-0.290	-0.370	4	121.7	7.12
31	0.793	-0.245	-0.250	-0.261	4	124.2	7.15
32	0.826	-0.261	-0.284	-0.289	4	123.0	7.17
33	0.839	-0.274	-0.258	-0.289	4	121.3	7.20*

* This is the selected estimate.

TABLE D-5

AZIMUTH ERROR ESTIMATION FOR 50-60 nmi RANGE INTERVAL

N	CORR (M-3)	CORR (M-2)	CORR (M-1)	CORR (M)	M	SIGMA (mrad)	TRACE
8	0.777	-0.390	-0.400	-0.345	3	0.541	4.00
9	0.852	-0.355	-0.440	-0.440	3	0.503	4.86
10	0.879	-0.361	-0.369	-0.402	3	0.476	5.65
11	0.895	-0.310	-0.395	-0.421	3	0.463	5.87
12	0.918	-0.302	-0.377	-0.439	3	0.451	6.07
13	0.935	-0.050	-0.196	-0.442	3	0.446	6.24
14	0.946	-0.052	-0.153	-0.412	3	0.439	6.37
15	0.956	-0.201	-0.261	-0.270	3	0.464	6.49
16	0.962	-0.195	-0.258	-0.270	3	0.461	6.60
17	0.967	-0.084	-0.080	-0.079	3	0.477	6.70
18	0.972	-0.055	-0.081	-0.080	3	0.484	6.78
19	0.973	-0.105	-0.102	-0.144	3	0.463	6.86
20	0.974	-0.022	-0.083	-0.163	3	0.457	6.93
21	0.065	-0.055	-0.056	-0.072	4	0.458	6.76
22	0.009	-0.067	-0.021	-0.021	4	0.432	6.82
23	0.026	-0.030	-0.013	-0.142	7	0.472	6.14
24	0.058	-0.025	-0.018	-0.121	5	0.467	6.66
25	0.057	-0.051	-0.051	-0.084	5	0.445	6.72
26	0.068	-0.055	-0.052	-0.072	5	0.443	6.77
27	0.053	-0.117	-0.115	-0.144	5	0.455	6.82
28	0.104	-0.116	-0.113	-0.142	5	0.452	6.87
29	0.035	-0.020	-0.127	-0.148	6	0.449	6.76
30	0.003	-0.077	-0.074	-0.147	6	0.430	6.80
31	0.300	-0.008	-0.145	-0.085	5	0.440	7.00
32	0.343	-0.051	-0.164	-0.152	5	0.445	7.03*
33	0.055	-0.219	-0.224	-0.245	6	0.433	6.91

* This is the selected estimate.

TABLE D-6

HEIGHT ERROR ESTIMATION FOR 50-60 nmi RANGE INTERVAL

N	CORR (M-3)	CORR (M-2)	CORR (M-1)	CORR (M)	M	SIGMA (FEET)	TRACE
8	0.051	-0.329	-0.396	-0.667	5	166.2	2.00
9	0.075	-0.160	-0.207	-0.609	5	209.7	3.00
10	0.085	-0.067	-0.084	-0.441	5	217.5	3.97
11	0.089	-0.007	-0.020	-0.282	5	220.3	4.59
12	0.026	-0.185	-0.211	-0.520	7	191.1	3.85
13	0.051	-0.106	-0.129	-0.378	7	199.4	4.30
14	0.044	-0.038	-0.054	-0.289	7	207.6	4.64
15	0.006	-0.002	-0.202	-0.233	8	221.2	4.50
16	0.001	-0.043	-0.013	-0.126	7	234.6	5.22
17	0.128	-0.007	-0.000	-0.007	5	237.9	6.07
18	0.007	-0.047	-0.050	-0.048	6	245.5	5.87
19	0.054	-0.057	-0.050	-0.097	5	233.8	6.28
20	0.019	-0.048	-0.085	-0.098	5	232.2	6.37
21	0.007	-0.052	-0.050	-0.149	5	231.6	6.45
22	0.604	-0.015	-0.058	-0.126	3	228.5	7.04
23	0.636	-0.047	-0.078	-0.122	3	230.8	7.09
24	0.547	-0.181	-0.241	-0.216	3	237.6	7.14
25	0.576	-0.196	-0.237	-0.225	3	236.6	7.18
26	0.542	-0.161	-0.274	-0.273	3	233.5	7.22
27	0.606	-0.108	-0.269	-0.264	3	231.9	7.25
28	0.539	-0.074	-0.283	-0.284	3	241.5	7.28
29	0.613	-0.003	-0.283	-0.271	3	240.9	7.31*
30	0.106	-0.285	-0.304	-0.383	4	236.3	7.12
31	0.106	-0.273	-0.310	-0.335	4	240.0	7.15
32	0.106	-0.191	-0.278	-0.276	4	242.3	7.17
33	0.106	-0.180	-0.219	-0.210	4	240.1	7.20

*This is the selected estimate.

To demonstrate that these estimates are truly consistent with the theory within the limits of sampling-induced uncertainty, consider that the sum of the two traces are 13.6, 14.2, and 14.3 for range, azimuth, and height respectively. Once again the square-root of the upper and lower 90% confidence bounds for the estimates are shown below as bracketing theory in all these cases.

RANGE

71.4 $\leq$ 114 ft $\leq$ 139

AZIMUTH

0.316 $\leq$ 0.4 mrad $\leq$ 0.600

HEIGHT

183 $\leq$ 310 ft $\leq$ 347

Figures D-3 through D-7 show the results for all legs included in this flight test (plotted in Figure D-2). Figure D-3 shows the probability of detection based on 10-nmi range intervals. Not until the size of the range intervals is reduced (Figure D-4) is multi-path interference observable. Figures D-5, D-6, and D-7 plot the averaged estimates for range, azimuth and height error respectively. These are the standard plotted outputs available from the statistics package constructed from the concepts introduced in this report.
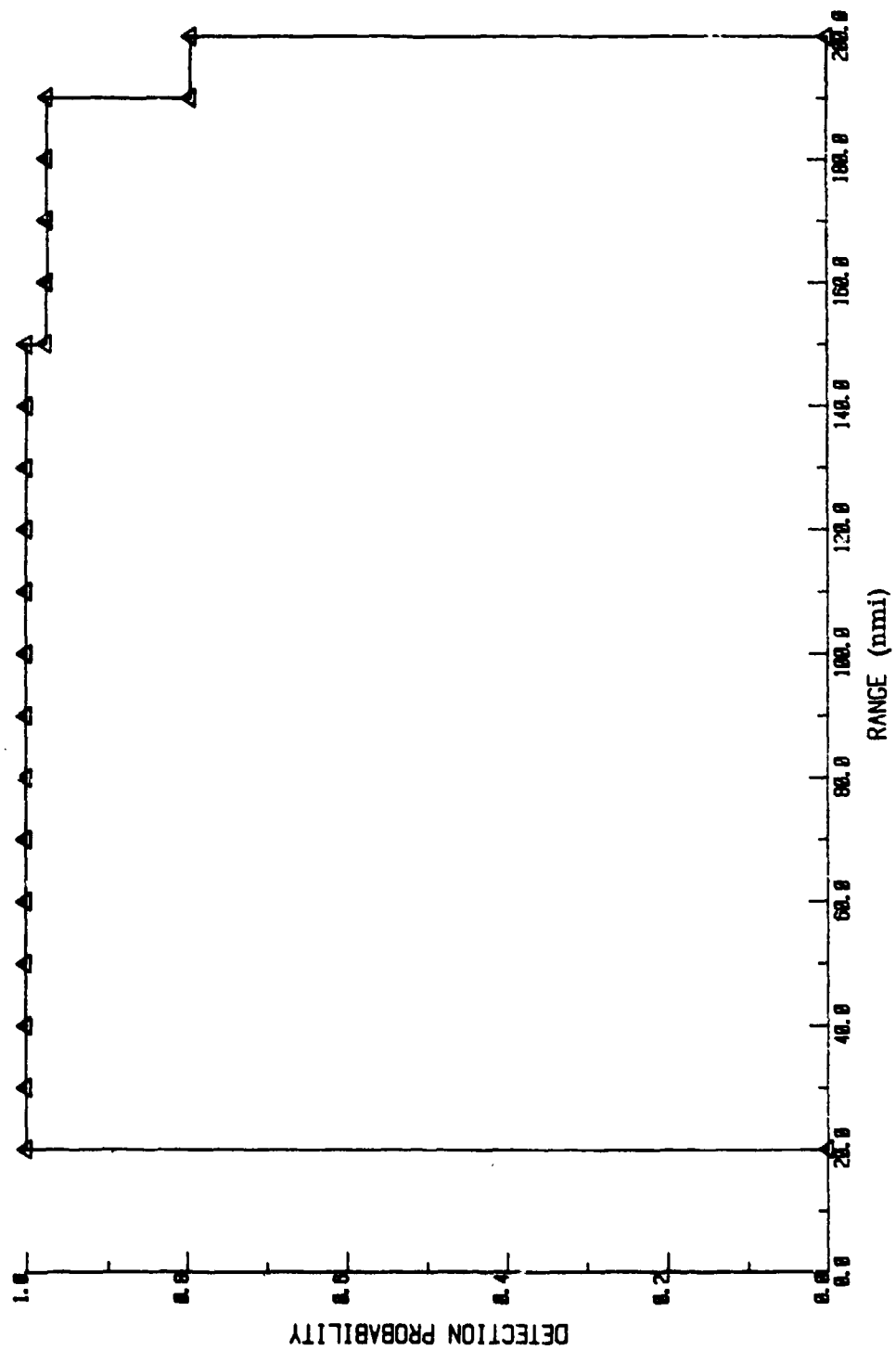
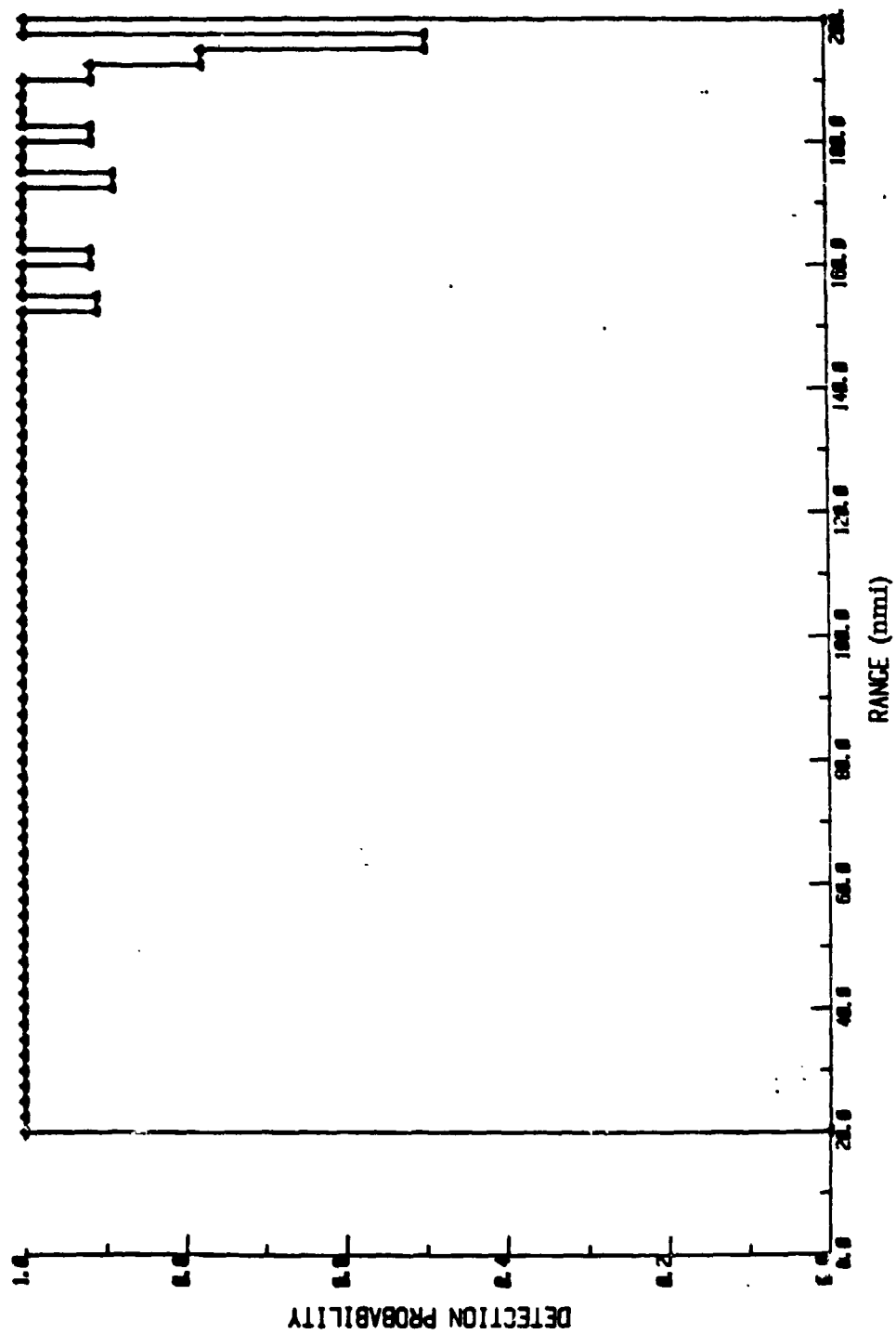Figure D-3. Probability of Detection Plot Demonstration

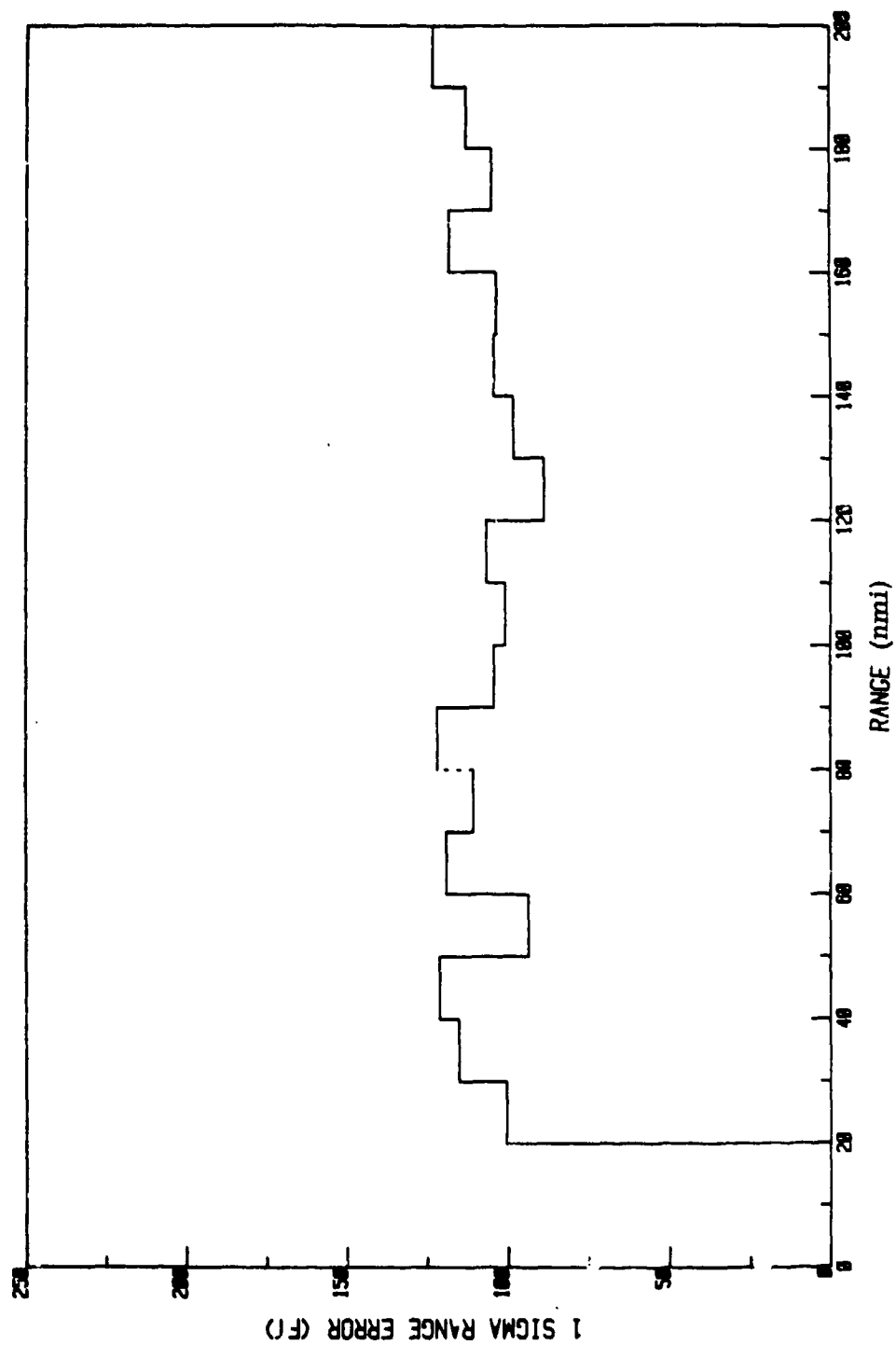Figure D-4. Probability of Detection Plot
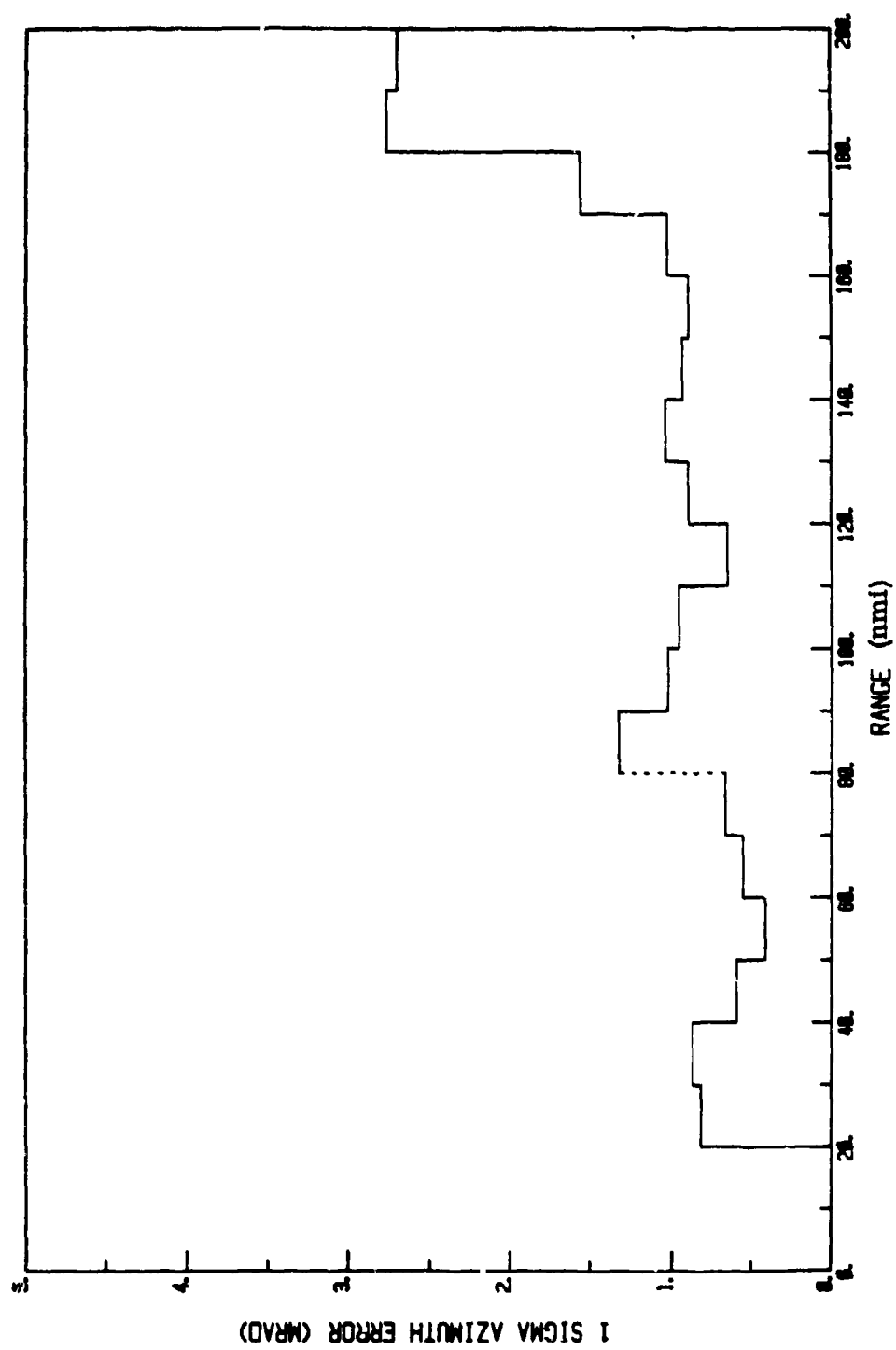
Figure D-5. Standard Deviation Plot Demonstration (Range)

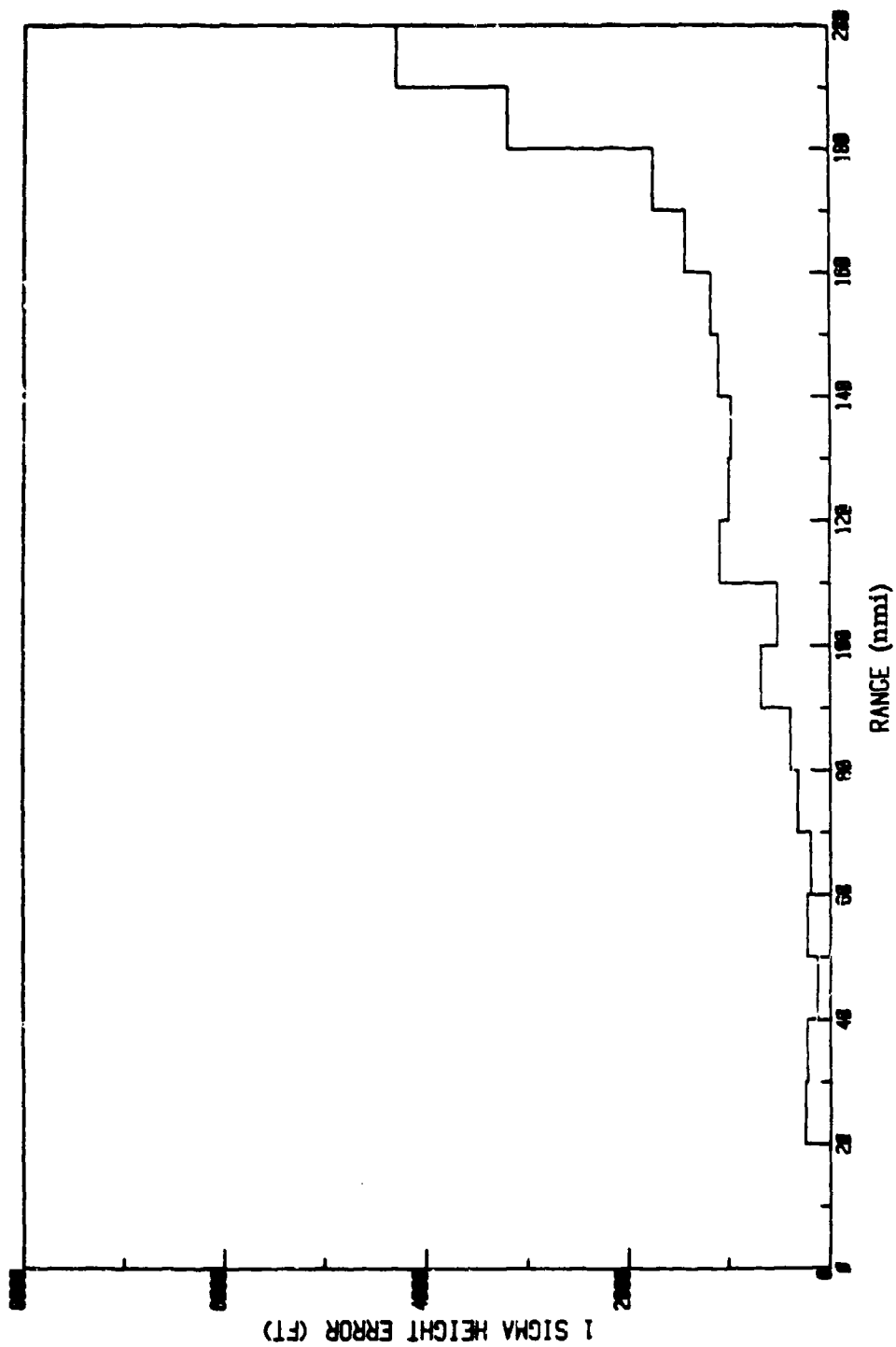Figure D-6. Standard Deviation Plot Demonstration (Azimuth)

D-14

Figure D-7. Standard Deviation Plot Demonstration (Height)

APPENDIX E

STATISTICAL COMPARISON OF RESULTS FROM A REAL-FLIGHT TEST
WITH A CO-LOCATED PRECISION REFERENCE STANDARD

This Appendix documents a recent opportunity to validate the autonomous technique by direct comparison with the results obtained by the more conventional method, i.e., using a precision reference standard.

Comparisons were made for approximately 6 flight legs for ranges between 20 and 200 nmi. A small aircraft flew closely controlled radial legs and the results for both techniques are presented for 20 nmi range bins in Figures E-1, E-2, and E-3 for the standard deviation of range, azimuth, and height respectively. The dark solid lines are the results for the autonomous method, while the lighter solid lines are the results from comparison with a precision reference standard. Both estimates are independent random variables because of the limited sample size (7 to 14 samples per range bin). Because these variance estimates are subject to sampling uncertainty, I have also shown 95% confidence bounds for both methods. The dotted lines are bounds for the autonomous method, while the dashed lines are bounds for the method using the reference standard. The cross-hatched areas represent regions of overlap. A reasonable interpretation is that if either estimate lies within an overlapped region, then the two estimates can be considered consistent with 95% confidence. Estimates for all three coordinates are consistent between the two methods for all nine range bins.
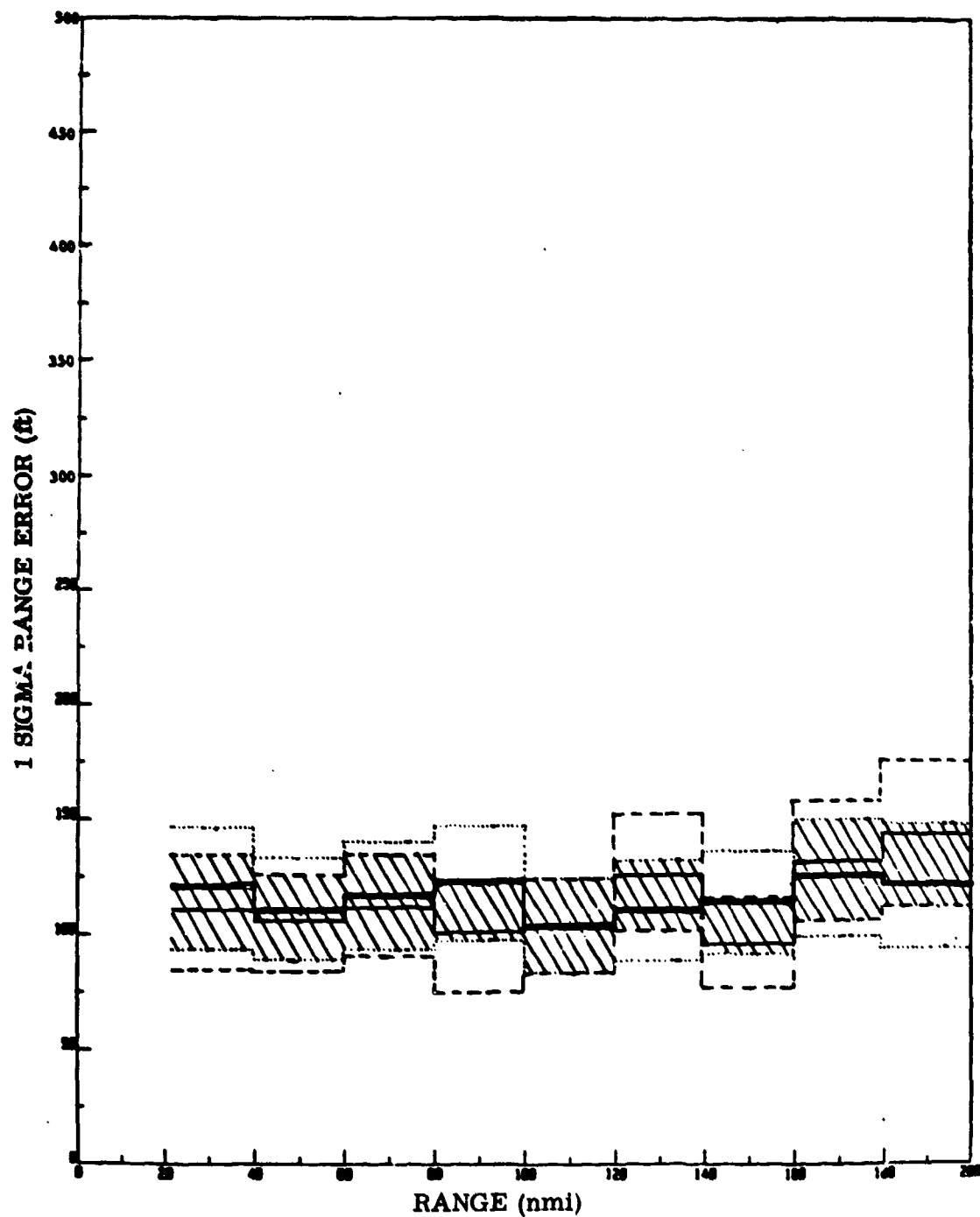
Figure E-1. Statistical Comparison of Direct Method to Autonomous
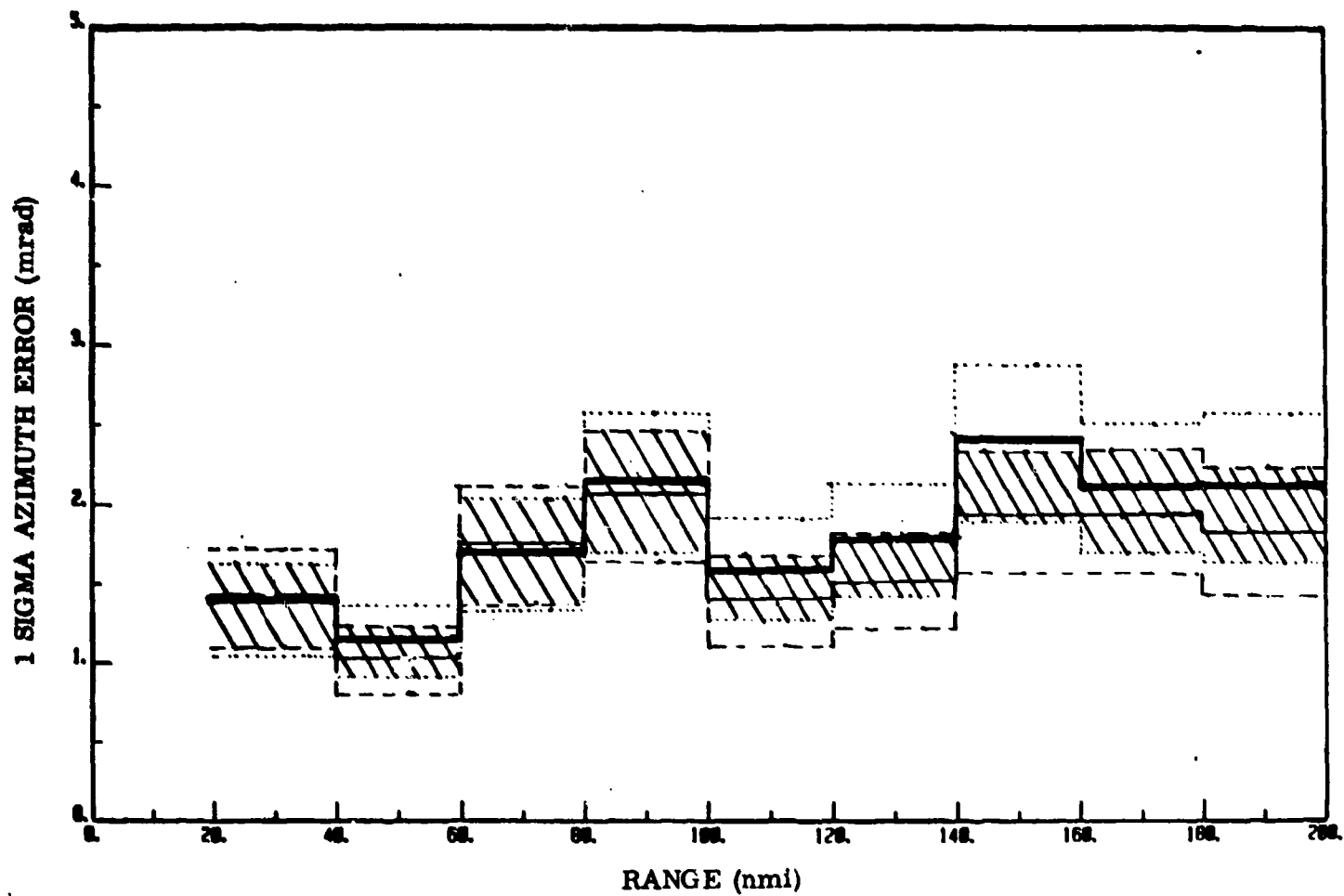Technique for Estimating 1 Sigma Range Error

Figure E-2. Statistical Comparison of Direct Method to
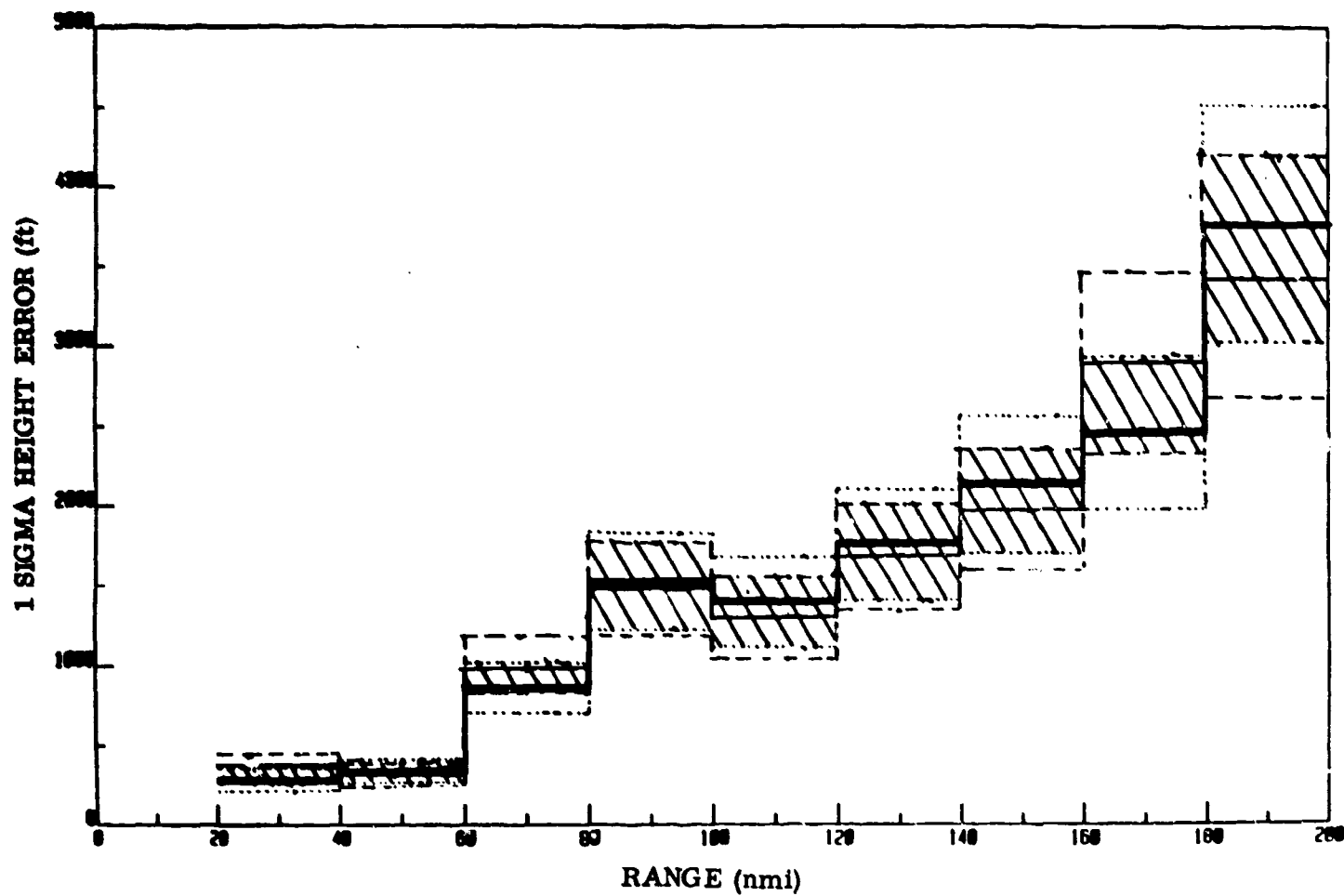Autonomous Technique for Estimating
1 Sigma Azimuth Error

Figure E-3. Statistical Comparison of Direct Method to
Autonomous Technique for Estimating
1 Sigma Height Error

APPENDIX F

AN EXAMPLE OF THE INVERSE CHARACTERISTIC FUNCTION
BY DISCRETE FOURIER TRANSFORMS

From par. 8.1, it was stated that inverse characteristic functions could be numerically computed from discrete Fourier transforms. Consider the Gamma distribution as an example,

$$g(t) = \frac{1}{\beta^a \Gamma(a)} \, t^{a-1} e^{-t/\beta}, \tag{F-1}$$

where

$$a = \nu/2, \tag{F-2}$$

and

$$\beta = 1/a, \tag{F-3}$$

and which has a characteristic function

$$\phi(\omega) = \left(\frac{a}{a - j\omega} \right)^a. \tag{F-4}$$

Suppose we have a random variable which is the sum of p gamma-distributed variates. Then the characteristic function of this sum is

$$\Phi_\Sigma(\omega) = \prod_{i \in p} \left(\frac{a_i}{a_i - j\omega} \right)^{a_i} \tag{F-5}$$

which has no known general inverse for arbitrary $\left\{ \nu_i \right\}$.

The distribution for the general sum can be obtained from the inverse characteristic function

$$g_\Sigma(t) = \int_{-\infty}^{\infty} \prod_{i\epsilon p} \left(\frac{\nu_i/2}{\nu_i/2 - j\omega}\right)^{\nu_i/2} e^{-j\omega t}\, d\omega. \qquad \text{(F-6)}$$

As a discrete Fourier transform,

$$\hat{g}_\Sigma(k) = \Delta\omega \sum_{n=0}^{N-1} \prod_{i\epsilon p} \left(\frac{\nu_i/2}{\nu_i/2 - j\omega_n}\right)^{\nu_i/2} e^{-j\omega_n k}, \qquad \text{(F-7)}$$

$$k = 0,\ 1,\ 2, \cdots\cdots N-1,$$

where t is a sample of the random variable $\hat{\sigma^2_\Sigma}/\sigma^2$ and we evenly sample all of t-space at least 2N times. Note that when all $\{\nu_i\}$ are equal for each leg that

$$\beta = \frac{2}{\nu}; \qquad a = p\,\nu/2 \qquad \text{(F-8)}$$

so that the distribution becomes gamma again with p Trace ν'_{22} degrees of freedom.

Figure F-1 shows the results of such a numerical inverse for N=4096 with ten legs, each having $\nu = 6$, so that $\beta = 1/3$ and $a = 30$. Here we have plotted the cumulative distribution, i.e. solid line, since this is the statistic important to risk and confidence considerations. The circles are samples of the theoretical gamma distribution with the same parameters. The agreement is excellent over the entire range of interest. To illustrate the error encountered by assuming that the sum $\sum_{i\epsilon p} \nu_i$ is the only parameter of importance, consider the second curve (dashed) in Figure F-1 which preserves the total number of degrees of freedom, i.e. 60, but which has different values of ν_i from leg-to-leg. The difference can be quite large. For example, if a producer's risk of 0.1% is desired, then the true pass/fail threshold would be $\sqrt{18.7}\ \sigma$ instead of the assumed threshold of $\sqrt{16.5}\ \sigma$, a difference of about 6.5%.
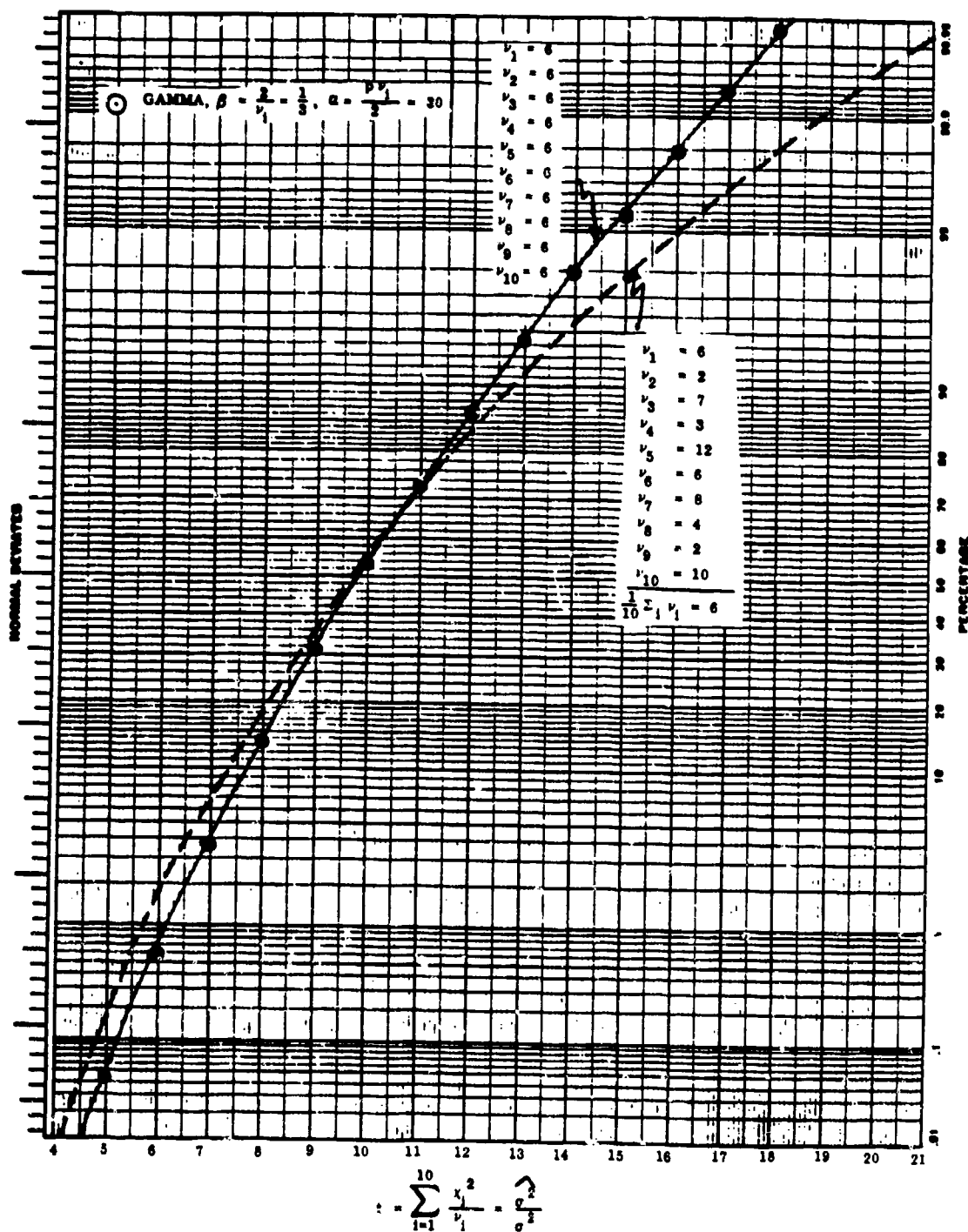
F-2

Figure F-1. Examples of Cumulative Distributions from Inverse Fourier Transforms

$$t = \sum_{i=1}^{10} \frac{x_i^2}{\nu_i} = \frac{\hat{\sigma}^2}{\sigma^2}$$

ENGLISH-METRIC/METRIC-ENGLISH CONVERSION TABLE

mm	=	0.1 cm	lb	=	453.6 g
cm	=	0.3937 in.	lb	=	0.4536 kg
cm	=	0.0328 ft	metric ton	=	1.12 tons (U.S.)
cm	=	10 mm			
cm^2	=	0.1550 in.^{2}	m	=	39.37 in.
cm^2	=	$1.076 \cdot 10^{-3}$ ft^2	m	=	3.281 ft
cm^3	=	0.061 in.^{3}	m	=	1.0936 yd
cm^3	=	$3.531 \cdot 10^{-5}$ ft^3	m^2	=	10.76 ft^2
			m^2	=	1.196 yd^2
ft	=	30.48 cm	m^3	=	35.32 ft^3
ft	=	0.3048 m	m^3	=	1.430 yd^3
ft^2	=	0.0929 m^2			
ft^2	=	929.37 cm^2	mi	=	1.6093 km
ft^2	=	$9.294 \cdot 10^{-3}$ km^2	mi	=	5280 ft
ft^3	=	0.0283 m^3	mi	=	0.87 nmi
			mi	=	1760 yd
in.	=	2.54 cm	mi^2	=	2.59 km^2
in.^{2}	=	6.452 cm^2	mi/h	=	0.87 knots
in.^{3}	=	16.387 cm^2			
			nmi	=	1.852 km
μm (micron)	=	0.001 mm	nmi	=	6076 ft
μm	=	10^{-6} m	nmi	=	1.15 mi
μm	=	10^{-4} cm			
μin.	=	$2.54 \cdot 10^{-5}$ mm	yd	=	0.9144 m
			yd^2	=	0.836 m^2
kg	=	2.2046 lbs	yd^3	=	0.7645 m^3
km	=	3281 ft	qt	=	0.946 liter
km	=	0.6214 mi	liter	=	1.057 qt
km	=	0.55 nmi	acre	=	43,560 ft^2
km^2	=	$1.076 \cdot 10^7$ ft^2	acre	=	4046.72 m^2
km^2	=	0.361 mi^2			
km/h	=	0.913 ft/s	rad	=	57.2958°
			deg	=	0.017 rad
knot	=	1.152 mi/h			
oz	=	28.35 g	°F	=	9/5(°C) + 32
oz	=	0.062 lbs	°C	=	5/9(F° − 32)

GENERAL ELECTRIC COMPANY TECHNICAL INFORMATION

Within the limitations imposed by Government data export regulations and security classifications, the availability of General Electric Company technical information is regulated by the following classifications in order to safeguard proprietary information:

CLASS 1: GENERAL INFORMATION

Available to anyone on request.
Patent, legal and commercial review
required before issue.

CLASS 2: GENERAL COMPANY INFORMATION

Available to any General Electric Company
employee on request.
Available to any General Electric Subsidiary
or Licensee subject to existing agreements.
Disclosure outside General Electric Company
requires approval of originating component.

CLASS 3: LIMITED AVAILABILITY INFORMATION

Original Distribution to those individuals with
specific need for information.
Subsequent Company availability requires
originating component approval.
Disclosure outside Gene... ' Electric Company
requires approval of originating component.

CLASS 4: HIGHLY RESTRICTED DISTRIBUTION

Original distribution to those individuals person-
ally responsible for the Company's interests in
the subject.
Copies serially numbered, assigned and recorded
by name.
Material content, and knowledge of existence,
restricted to copy holder.

GOVERNMENT SECURITY CLASSIFICATIONS, when required, take precedence
in the handling of the material. Wherever not specifically disallowed, the General
Electric classifications should also be included in order to obtain proper handling
routines.